SLAC-28
UC-28, Particle Accelerators
and High-Voltage Machines
UC-34, Physics
TID-4500

A PULSED BENDING MAGNET FOR THE BEAM SWITCHYARD AREA OF THE STANFORD TWO-MILE LINEAR ELECTRON ACCELERATOR

May 1964

by

H. Brechna

Technical Report
Prepared Under
Contract AT(04-3)-400
for the USAEC
San Francisco Operations Office

Printed in USA. Price $2.00. Available from the Office of Technical Services, Department of Commerce, Washington 25, D.C.

ABSTRACT

This paper presents the results of detailed calculations and the design of a switching or pulsed magnet. The magnet has a laminated H-type core and a multistranded water-cooled coil, and is suitable for bending an electron beam of 25 GeV/c an angle of $\pm 0.5^{\circ}$. The switching magnet is located in the beam switchyard area of the Stanford two-mile linear accelerator. Problems concerning the laminated core and the multistranded coil, the ac losses, the temperature rise, and the effect of pole shaping on field homogeneity in the gap are treated.

The design parameters of an inductive load to be used in connection with the pulsed magnet are given in brief. The noise level and the core losses for the magnet are calculated.

The design of the magnet for an energy level of 25 GeV/c electrons may seem conservative but it was determined that the magnets should work also for an energy of 40 GeV/c electrons representing a later stage of the linear accelerator operation.

TABLE OF CONTENTS

LIST OF FIGURES

LIST OF SYMBOLS

a constant depending on core configuration; distance from hot-spot to core surface

A effective core cross section

b constant depending on core configuration; coil height

B magnetic field

B_o = flux density well inside the gap

c spacing between centers of adjacent turns

c_p = specific heat

C capacitance, constants

C_{Nu} = Nusselt number; C_{GR} = Groshof number; C_{PR} = Prandtl number

d pulse length

d_o = cable diameter bare

d_{ins} = insulation thickness

d_h = hydraulic diameter

d_s = diameter of individual strands in a conductor

D overall coil width

D_c cable diameter

E energy

f frequency

g half gap height

G function of conductor diameter to calculate ac losses

h distance between pole surface and yoke

h' distance pole end to mirror

h_1 heat transfer coefficient

H function of conductor diameter to calculate ac losses. Magnetization force

i current (instant value)

I current; ignitron

I_p = peak current; I_{av} = average; I_{rms} = mean square root

IN ampere turns

IN_g gap ampere turns

IN_{tot} total ampere turns

k constants depending on n; heat conductivity

$k_1 = \frac{g}{h}$

$k_2 = \frac{B_y}{B_o}$

$k_3 = B_x \cdot \frac{h}{V_o}$

ℓ length

ℓ_{eff} = effective magnetic field length

ℓ_h = hydraulic length

ℓ_m = mean turn length

ℓ_{Fe} = length of homogeneous field inside gap along z-axis

L noise level; inductance

m number of pancakes

n number of strands in cable

Fourier coefficient

N number of turns

p loss density; pressure

p_{Fe} = core loss density

p'_{Fe} = corrected core loss density for oriented sheets

Δp = pressure drop

P losses

P_{Fe} = core losses

P_{av} = average losses

P_p = peak value

Q quality factor

Q_h = amount of coolant

r flux penetration depth in core (used in IV.B.1)

R resistance

R_M = magnet resistance

$R_\sim$ = ac resistance

$R_=$ = dc resistance

s change in gap height due to saturation in iron (used in IV.B.1)

t time; transformed coordinate; coil width

t_p = pulse time

T period between successive pulses

U flux; voltage

U_o = applied voltage

V field volume; potential

V_o = pole surface potential

w power density; pole width

w_V = power density per unit volume (watts/cm^3)

w_s = power density per unit area (watts/cm^2)

W potential function

z coordinate

Z impedance

$Z_o = (L/c)^{\frac{1}{2}}$

Z_{eff} = effective impedance

α angle of tapering of pole ends

flux deviation from rolling direction

β volume expansion coefficient

γ core sheet density

Δ distance between mirrors

κ conductor conductivity; coil factor

λ pole shape parameter; fill factor

μ permeability; viscosity

μ_o permeability of air

ν kinematic viscosity

ρ resistivity

Φ flux

θ temperature

θ_b = bulk temperature

θ_w = wall temperature

$\Delta\theta$ = temperature rise

$\Delta\theta_i$ = temperature rise in core

$\Delta\theta_o$ = temperature rise in boundary layers

θ_s = hot-spot temperature

I. GENERAL

The purpose of the pulsed magnet is to bend the electron beam, coming from the two-mile linear accelerator with a repetition rate of 360 pulses per second or less, into three different channels.

To bend an electron beam of 25 GeV/c through an angle of $\pm 0.5^{\circ}$ we must have

$$\int_0^z Bdz = 0.73 \text{ (weber/meter)} \tag{I.1}$$

In order to avoid either a long magnet or high flux density in the gap, the magnet length was split into five equal units, each having an effective length of 0.85 meter and deflecting the beam $\pm 0.1^{\circ}$. This division gave more flexibility in the manufacturing of the individual magnets as well as a simplification in maintenance and service. The position of the five magnets along the beam leads to an axial field distribution, as shown schematically in Fig. 1.

Each magnet is equipped with magnetic mirrors (2) and the actual distance between mirrors is taken to be Δ. The half-width of the gap is denoted by g. By appropriate shimming (see Section III), the axial field distribution gives the relation

$$\int_0^z Bdz \approx 5(0.8 + 2g)B_o \tag{I.2}$$

where B_o indicates the flux density in the symmetry axis of the magnet well inside the gap.

With $2g$ chosen to be 5 cm, Eqs. (I.1) and (I.2) yield

$$B_o = 0.17 \text{ (weber/meter}^2\text{)}$$

A more accurate calculation of $\int Bd\ell$ to fit the experimental curves of B_y in the fringing field area for our particular application is given

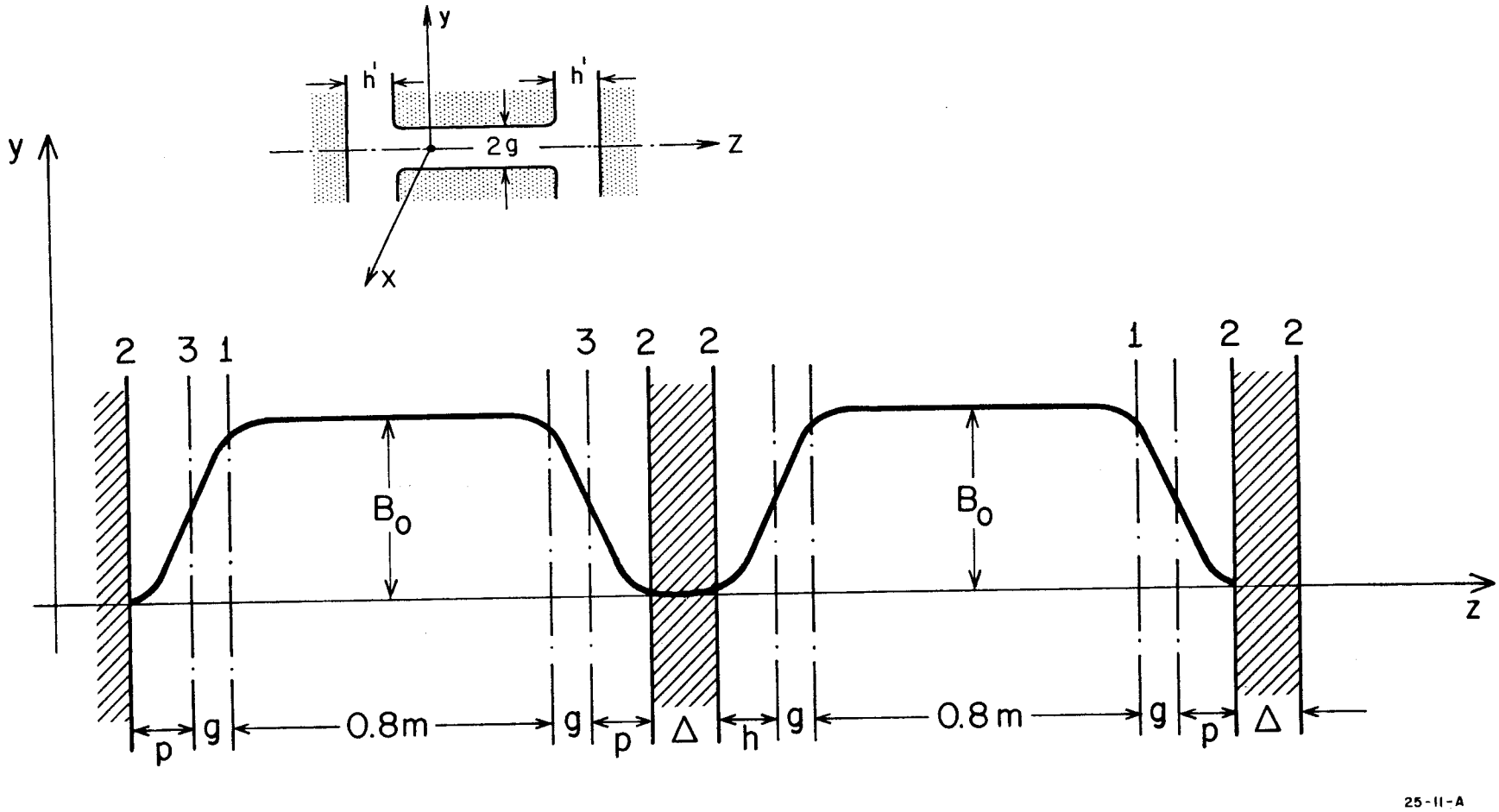

FIG. 1--Field distribution along the beam.

1. Position of the pole edge
2. Position of magnetic mirror
3. Virtual field boundary

2g - gap width

Δ - axial distance between mirrors of successive magnets

in Section III.B and III.C. The aberration caused in the beam by the magnet must be small compared to the emittance of the beam coming from the accelerator. To have a homogeneous field of $\Delta B/B \approx 10^{-4}$ over a range of ±2 cm around the center of the beam, the pole width of the pulsed magnet is chosen to be 16 cm and the pole ends are shimmed according to the detail shown in Fig. 2.

The field energy required for bending the electron beam is

$$E_m = \tfrac{1}{2} \int HB dV$$

or

$$E_m = 0.5(I_p N)\Phi \tag{I.3}$$

The peak energy is calculated to be

$$E = 106 \text{ joules}$$

The pulser frequency was chosen to be 1000 sec^{-1}. The pulse duration (neglecting for the first approximation the coil and equivalent core resistance) is

$$t_p = 2\pi \sqrt{LC} \tag{I.4}$$

Because

$$E = \frac{CU^2}{2} = \frac{LI^2}{2} \tag{I.5}$$

with the peak voltage across the magnet terminals chosen to be

$$U = 4200 \text{ volts}$$

it is found from Eqs. (I.4) and (I.5) that

$$C = 12.0 \times 10^{-6} \text{ farad}$$

$$L = 2.1 \times 10^{-3} \text{ henry}$$

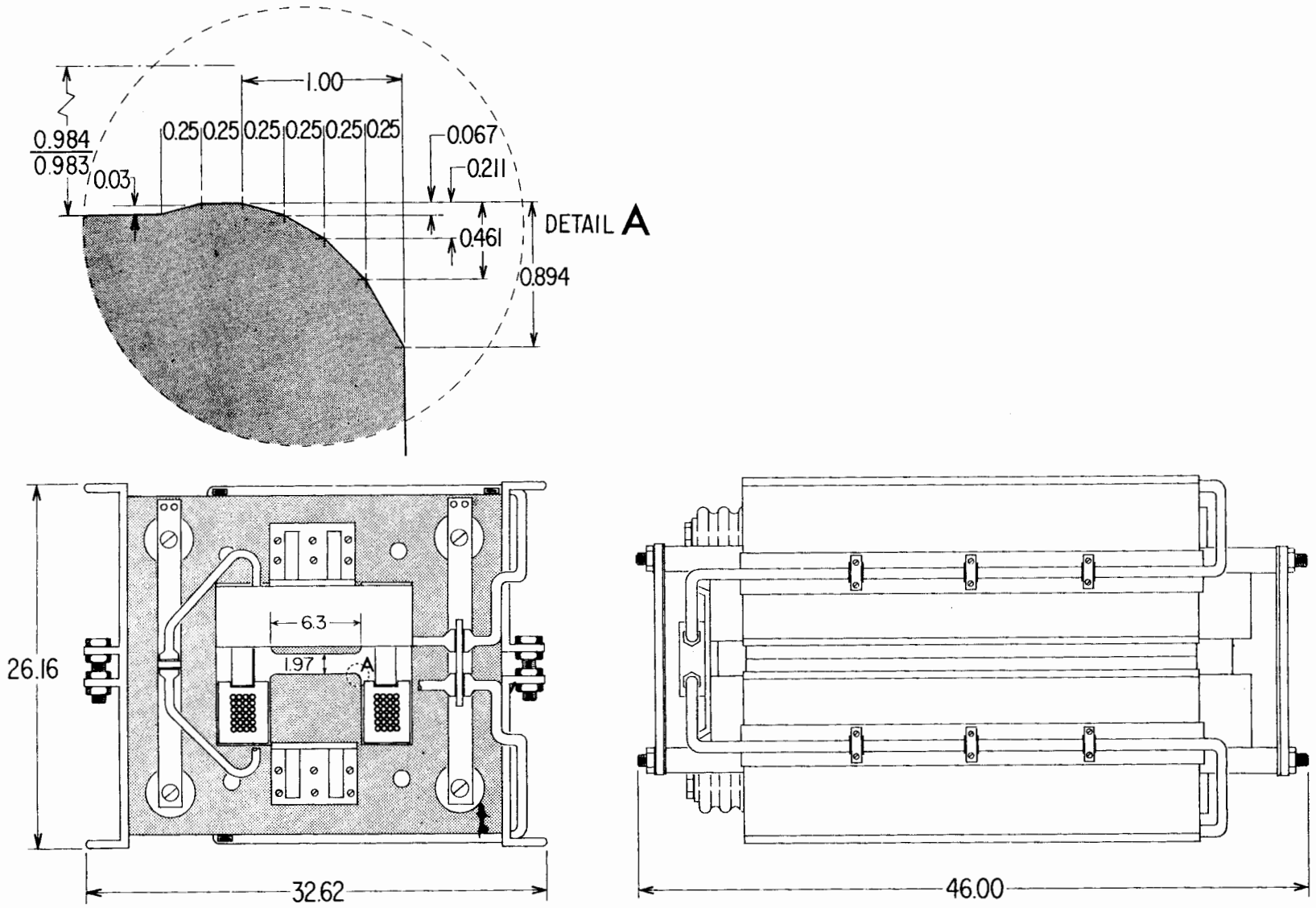

FIG. 2--Pulsed magnet main dimensions.

and the peak current is

$$I_p\Big|_{R=0} = 318 \text{ amperes}$$

The peak ampere-turns of the gap calculated are:

$$\mathbb{N}_\delta = (0.8)B_o\delta$$

$$\approx 7000 \text{ ampere-turns} \qquad (I.6)$$

The total number of ampere-turns for one pulsed magnet is (see Section IV)

$$\mathbb{N}_{tot} = 7200 \text{ ampere-turns}$$

The number of turns was chosen to be

$$N = 24$$

and the dc equivalent current is

$$I_p\Big|_{R\neq 0} = 300 \text{ amperes}$$

The coils are connected electrically in parallel. Figure 3 shows the coil configuration. It is also possible to wind two conductors parallel and to connect the coils in series. Both solutions are essentially equivalent. Using water-cooled cables (Section IV) with a conductor cross section of 8.3×10^{-5} meter^2 and the core dimensions given in Fig. 2, one obtains the magnet parameters given in Table I.

The pulser circuit shown in Fig. 4 was described in detail by J. Cole et al.[1]; its operation is repeated briefly below.

The pulser circuit energizing the pulsed or switching magnet P_M utilizes high voltage ignitrons (I) and inductances (L_1 and L_2).

The capacitor C_1 is charged by the power supply PS_1 to a chosen voltage. The capacitor is discharged through I_1 into the pulsed magnet

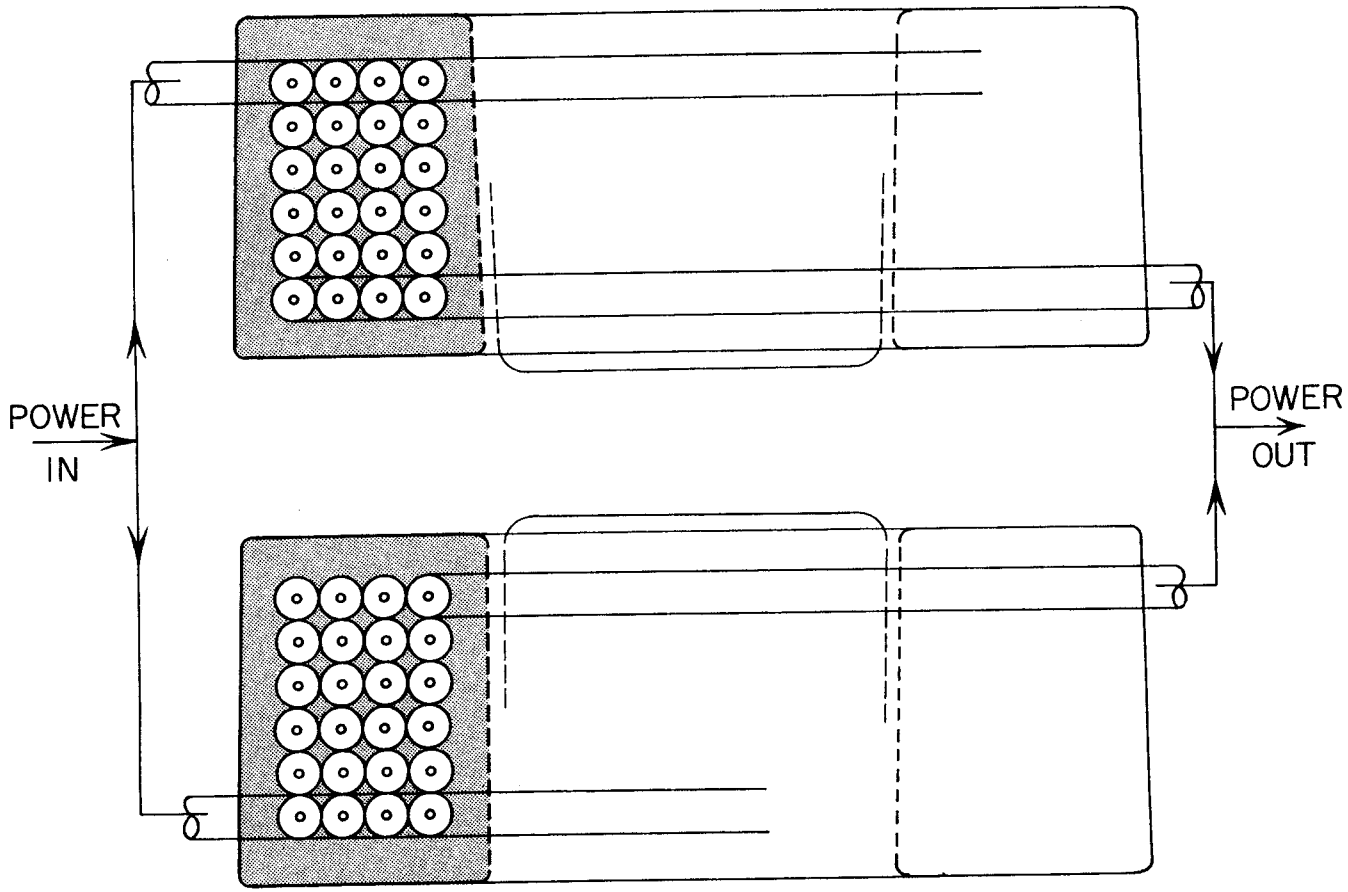

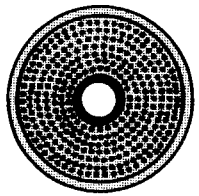

FIG. 3--Coil configuration. The two pole coils are connected electrically in parallel, and hydraulically in series. Around a soft copper core are wound individually insulated copper strands.

TABLE I

PULSED MAGNET (CALCULATED VALUES)

Electron beam energy	25 BeV
Beam bending angle per magnet	0.1^{o}
Flux density in gap (25 GeV electrons)	0.17 weber/meter^2
Effective magnet length	0.85 meter
Total magnet length	1.17 meter
Gap height	0.05 meter
Gap width	0.16 meter
Total ampere-turns (peak)	7600
Number of turns per pole (coils parallel)	24
Peak current (coils parallel, R $\equiv$ 0)	316 amperes
Peak voltage	4200 volts
Pulse frequency	1000/sec
Peak energy	106 joules
Conductor cross section	8.3×10^{-5} meter^2
DC coil resistance	6.5×10^{-3} ohms
Total coil resistance	1.65×10^{-2} ohms
Equivalent core resistance	5.3×10^{-2} ohms
Magnet inductance	$2.1 \cdot 10^{-3}$ henry (meas. 2.4×10^{-3} Hy)
Total ohmic losses in coil	150 watts
Total core losses	477 watts
Q value = $\frac{4\pi f E_m}{P_m}$	$\approx$ 190
Amount of cooling water	0.72 liter/minute
Water temperature rise through coil(average)	3.4^{o}C
Water temperature rise through core(average)	4.6^{o}C + 4.6^{o}C = 9.2^{o}C
Water pressure drop over magnet	5 kg/cm
Weight of coil	85 kg
Weight of core	1500 kg
Total weight	$\approx$ 1800 kg

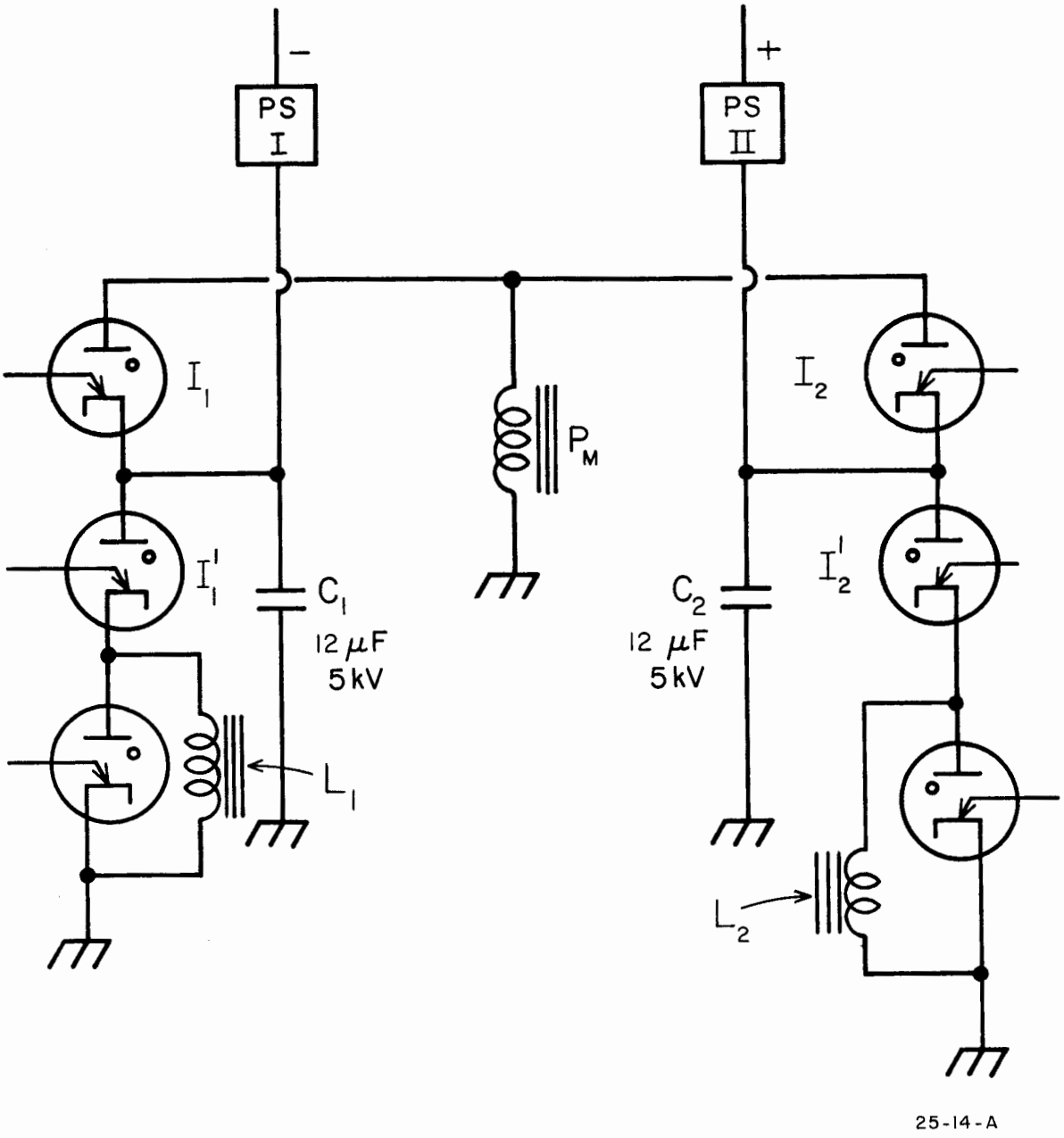

FIG 4--Pulser diagram. The pulsed magnet P_M may be energized either from power supply PS_I or PS_{II} according to the experimental setups in the end stations.

(P_M). The pulsed current flows through the magnet for half a cycle. During this half cycle the voltage over C_1 reverses. At the end of the half cycle, I_1 stops conducting, and I_1' is triggered. The capacitor C_1 is now discharged over L_1, which again causes polarity change of the capacitor. At the end of a full cycle C_1 is returned to its original polarity, but due to losses in the ignitrons, magnet, inductance, and leads, its voltage is recovered only partially. In order to make the circuit efficient, the voltage across the magnet terminals was chosen to be high as compared to the total voltage drop; a peak voltage of 4200 volts seemed to be a good compromise. From experience we know that 92% of the full voltage is recovered. The remaining charge is now supplied by PS_1, which charges C_1 to its original voltage.

Part II of the pulser circuit produces voltage of positive polarity and operates in the same manner as Part I.

The currents and voltages across the magnet and the capacitor are shown in the oscillograms, Fig. 5a and Fig. 5b.

II. MAGNET DISCHARGE PARAMETERS

In Section I the magnet equivalent resistance was, compared to the reactance, neglected. For this calculation the magnet resistance is considered. The magnet impedance is

$$Z_m = R_m + j\omega L_m \qquad \text{(II.1)}$$

After the ignitron I_1 (Fig. 4) is conducting, the current flowing through the magnet is

$$I(t) = I_p(e^{-\delta t})e^{j(\omega t - \varphi)} \qquad \text{(II.2)}$$

with

$$\delta = \frac{R_m}{2L_m}$$

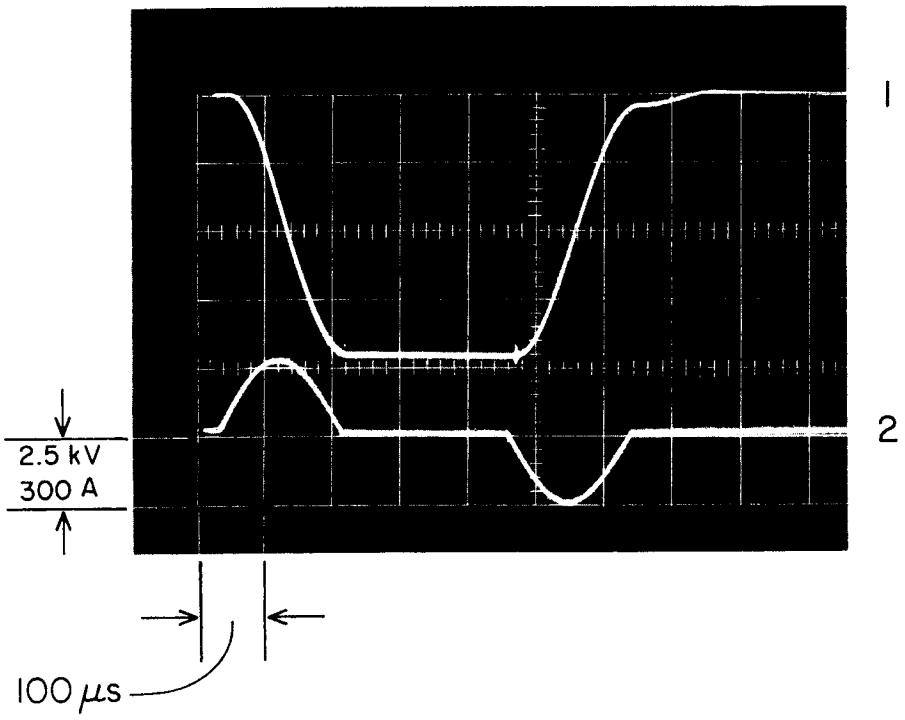

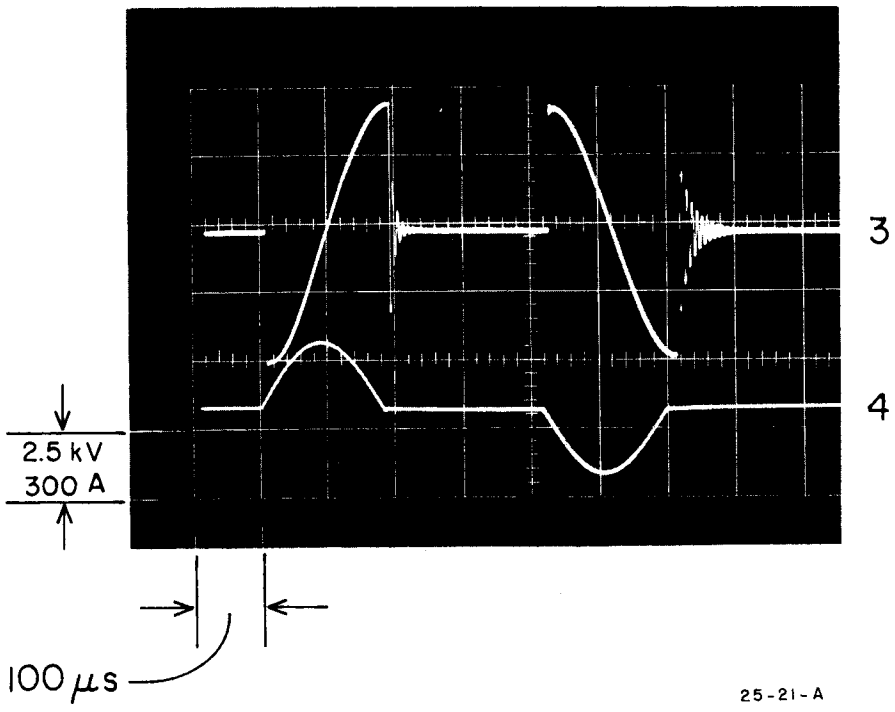

FIG. 5a and 5b--Voltage and current oscillograms of the capacitor and the magnet.

1. Capacitor voltage
2. Current through the capacitor
3. Voltage distribution of magnet
4. Current through magnet

and

$$I_p\Big|_{R\equiv 0} = U_o(C/L)^{\frac{1}{2}} = U_o/Z_o \qquad \text{(II.3)}$$

The real part of the current is

$$I(t) = U_o(C/L)^{\frac{1}{2}} \frac{e^{-\delta t_p}}{\left(1 - \frac{R^2C}{4L}\right)^{\frac{1}{2}}} \sin(\omega t) \qquad \text{(II.4)}$$

with

$$t_p = \frac{\pi}{2}(LC)^{\frac{1}{2}}$$

The effective magnet impedance may be expressed as

$$Z_{eff} = \left[\frac{L}{C}\left(1 - \frac{R^2C}{4L}\right)\right]^{\frac{1}{2}} e^{\frac{\pi R}{4(L/C)^{\frac{1}{2}}}} \qquad \text{(II.5)}$$

and the angular frequency as

$$\omega = \frac{1}{(LC)^{\frac{1}{2}}}\left(1 - \frac{R^2C}{4L}\right)^{-\frac{1}{2}} \qquad \text{(II.6)}$$

Using the magnet parameters given in Table I, one obtains

$$Z_o = 13.25 \text{ ohms}$$

$$Z_{eff} = 13.3 \text{ ohms}$$

$$\omega = 6.25 \times 10^{-3} \ (\text{sec}^{-1})$$

$$I(t) = 318\ e^{-1.61t} \sin(\omega t)$$

The peak current I_p is obtained at $t \approx \frac{1}{2}\pi(LC)^{\frac{1}{2}}$. Hence

$$I_p = U/Z_{eff} = 316 \text{ amperes.}$$

The effects of other circuit elements (L and R) have not been taken into consideration in this calculation, but they can be included in Eqs. (II.1) to (II.6).

III. FIELD DISTRIBUTION AND POLE FACE SHAPING

A. Field Distribution Near the Edge of a Rectangular Pole

The field near the edge of rectangular poles has been investigated by many authors. In a recent paper, Hedin[2] has treated this problem in detail. In this chapter a more simplified field calculation based on Hedin's work, using Schwartz-Christoffel conformal transformation, is given.

The iron saturation in the pole edges is neglected, and the pole and yoke configuration are shown in Fig. 6a. The saturation effect can be taken into consideration by the relation (IV.B.1), where B_{in} indicates the flux density in the iron, μ its permeability, and B_{out} the flux density in the gap, and s the extended gap due to saturation. The exciting coil is assumed to be far off and does not affect the field distribution. Due to the symmetry of the configuration, half the pole and gap in the z-plane is considered. The boundary line BCD has the magnetic potential V_o, and the lines BAD the potential 0. The real axis of the t-plane is transformed in the z-plane, with the pairs of corresponding points to be

C:	$z = jg$	$t = -1$
B:	$z = j$	$t = 0$
A:	$z = -h$	$t = a$

The Schwartz-Christoffel transformation leads to

$$\frac{dz}{dt} = C_1 (t+1)^{\frac{1}{2}} t^{-1} (t-a)^{-\frac{1}{2}} \qquad \text{(III.A.1)}$$

$$Z = C_1 \int \frac{(t+1)^{\frac{1}{2}}}{(t-a)^{\frac{1}{2}}} \cdot \frac{dt}{t} + C_2 \qquad \text{(III.A.2)}$$

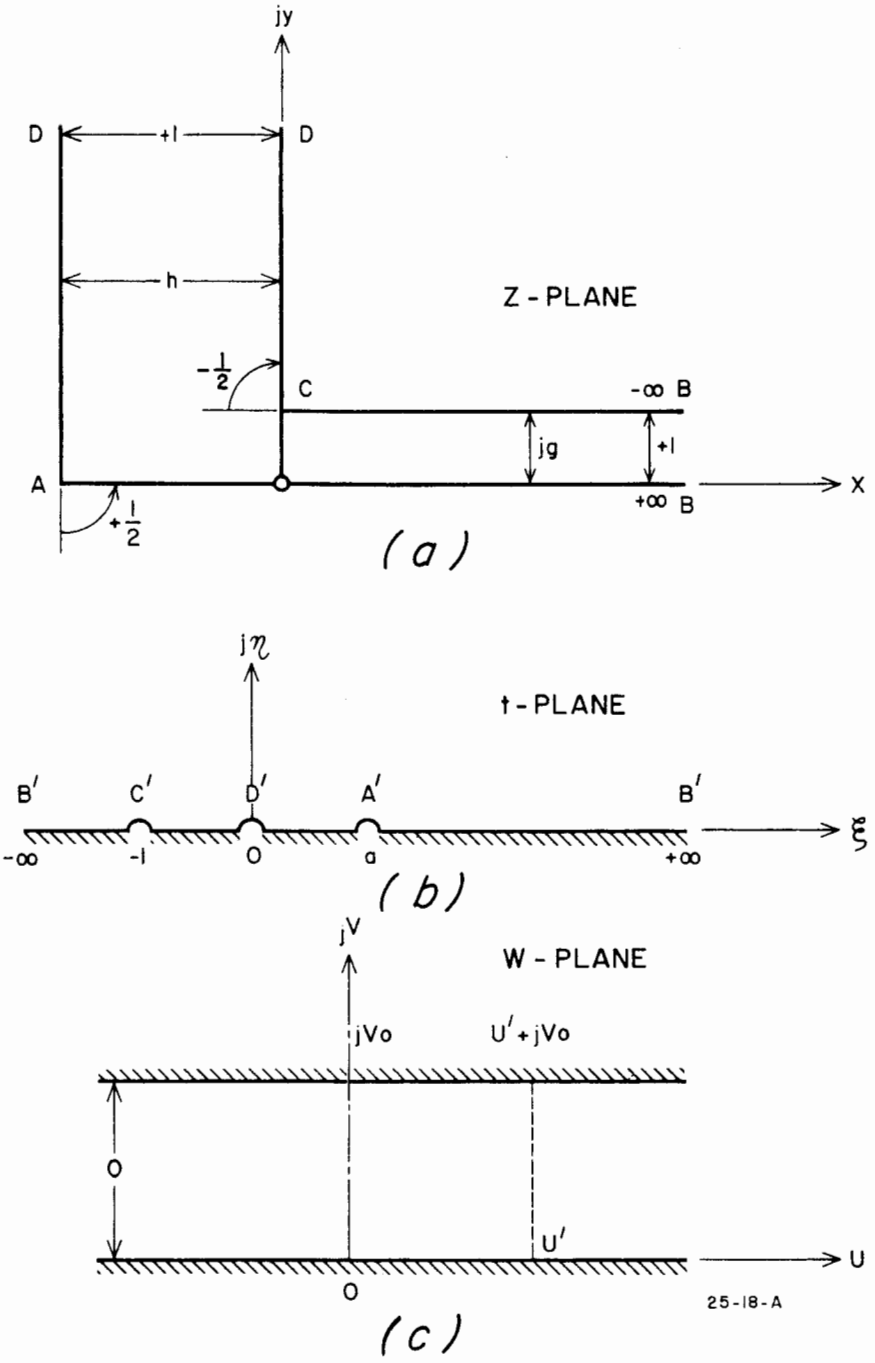

FIG. 6--Pole and yoke configuration.

(a) Schematic configuration of the pole and yokes.

(b) The upper half of the t-plane is transformed into the z-plane. The indicated points in t- and z-planes are corresponding.

(c) The t-plane is transformed in the w-plane. The boundary line BCD has the potential $V = V_0$, and the line BAD the potential $V = 0$.

Substituting

$$u = \left(\frac{t + 1}{t - a}\right)^{\frac{1}{2}}$$

yields

$$z = 2C_1 \int \frac{u^2(a + 1)}{(u^2 - 1)(au^2 + 1)}\, du + C_2$$

or

$$z = -2C_1\left[\int \frac{du}{u^2 - 1} + \frac{1}{a}\int \frac{du}{u^2 + \frac{1}{a}}\right] + C_2$$

Thus, by integration,

$$z = C_1 \ln \frac{u + 1}{u - 1} - \frac{2C_1}{\sqrt{a}} \cdot \tan^{-1}\left(u\sqrt{a}\right) + C_2$$

$$z = C_1 \ln \frac{\left(\frac{t + 1}{t - a}\right)^{\frac{1}{2}} + 1}{\left(\frac{t + 1}{t - a}\right)^{\frac{1}{2}} - 1} - \frac{2C_1}{\sqrt{a}} \cdot \tan^{-1}\left(\frac{a(t + 1)}{t - a}\right)^{\frac{1}{2}} + C_2 \qquad \text{(III.A.3)}$$

The integration constants C_1 and C_2 and the transformation constant a are best evaluated by the method of residues. For

$$z(t = a) = - h$$

$$z(t = -1) = jg$$

one obtains

$$C_1 = \frac{g}{\pi}; \qquad C_2 = 0; \qquad a = (g/h)^2$$

After some modifications, Eq. (III.A.3) becomes

$$z = \frac{g}{\pi} \ell n \left[\frac{\left(\frac{1 + \frac{1}{t}}{1 - \frac{a}{t}} \right)^{\frac{1}{2}} + 1}{\left(\frac{1 + \frac{1}{t}}{1 - \frac{a}{t}} \right)^{\frac{1}{2}} - 1} \right] - \frac{2h}{\pi} \tan^{-1} \left(\frac{t + 1}{\frac{t}{a} - 1} \right)^{\frac{1}{2}} \qquad \text{(III.A.4)}$$

For different parts of the polygon in the z-plane, different t-values are obtained. Over BC: $-\infty < t < -1$, Eq. (III.A.4) is modified to

$$z = jg + \frac{g}{\pi} \cdot \ell n \left[\frac{1 + \left(\frac{1 + \frac{1}{t}}{1 - \frac{a}{t}} \right)^{\frac{1}{2}}}{1 - \left(\frac{1 + \frac{1}{t}}{1 - \frac{a}{t}} \right)^{\frac{1}{2}}} \right] - \frac{2h}{\pi} \tan^{-1} \left(\frac{t + 1}{\frac{t}{a} - 1} \right)^{\frac{1}{2}} \qquad \text{(III.A.5)}$$

For $h \gg g$ (always true for magnets),

$$\tan^{-1} \left(\frac{t + 1}{\frac{t}{a} - 1} \right)^{\frac{1}{2}} = \tan^{-1} \left(\frac{1 + \frac{1}{t}}{\frac{1}{a} - \frac{1}{t}} \right)^{\frac{1}{2}} \approx \left(\frac{1 + \frac{1}{t}}{\frac{1}{a} - \frac{1}{t}} \right)^{\frac{1}{2}}$$

$$z \approx jg + \frac{g}{\pi} \ell n \left[\frac{1 + \left(1 + \frac{1}{t} \right)^{\frac{1}{2}}}{1 - \left(1 + \frac{1}{t} \right)^{\frac{1}{2}}} \right] - \frac{2g}{\pi} \left(1 + \frac{1}{t} \right)^{\frac{1}{2}} \qquad \text{(III.A.6)}$$

Over CD: $-1 < t < 0$,

$$z = jg + \frac{g}{\pi} \ell n \left[\frac{1 + j \left(- 1 - \frac{1}{t} \right)^{\frac{1}{2}}}{1 - j \left(- 1 - \frac{1}{t} \right)^{\frac{1}{2}}} \right] - \frac{2g}{\pi} j \left(- 1 - \frac{1}{t} \right)^{\frac{1}{2}}$$

from

$$\ell n \frac{1 + jp}{1 - jp} = 2j \tan^{-1} p$$

Thus

$$z = jg + 2j \frac{g}{\pi} \tan^{-1} \left(- 1 - \frac{1}{t}\right)^{\frac{1}{2}} - \frac{2g}{\pi} j\left(- 1 - \frac{1}{t}\right)^{\frac{1}{2}} \qquad \text{(III.A.7)}$$

To obtain the field distribution in the z-plane, it is necessary to have the potential V_o along the part of the t-axis between $-\infty$ and 0 and a potential zero in the part of the t-axis between 0 and $+\infty$. By transforming now the t-plane into a W-plane,

$$\frac{dW}{dt} = C_1 (t - 0)^{-1} \qquad \text{(III.A.8)}$$

$$W = \frac{V_o}{\pi} \ell nt \qquad \text{(III.A.9)}$$

where the potential function (Fig. 6c) is

$$W = U + jV$$

The potential is calculated for

$$x = 0 \qquad y = y_1 \gg g$$

$$t \to 0 \qquad \frac{1}{t} \gg 1$$

From Eq. (III.A.7),

$$jy_1 = jg - jg - \frac{2jg}{\pi} \cdot \sqrt{- \frac{1}{t}}$$

or

$$t = -\left(\frac{2g}{\pi y_1}\right)^2 \qquad \text{(III.A.10)}$$

Combining Eqs. (III.A.9) and (III.A.10) yields

$$U_1 = \frac{2V_o}{\pi} \ell n \left(\frac{2g}{\pi y_1}\right) \qquad \text{(III.A.11)}$$

For the point $y_2 = g$, with $x = x_2 \gg g$, the expression for $t \to -\infty$ and Eq. (III.A.6) is

$$x_2 = \frac{g}{\pi} [2 \ell n\, 2 + \ell n t - 2]$$

and

$$U_2 = \frac{V_o}{\pi}\left[2 - 2 \ell n\, 2 + \frac{\pi x_2}{g}\right] \qquad \text{(III.A.12)}$$

From Eqs. (III.A.11) and (III.A 12),

$$U_2 - U_1 = V_o\left[\frac{2}{\pi} - \frac{2}{\pi} \ell n \frac{4}{\pi} + \frac{x_2}{g} + \frac{2}{\pi} \ell n \frac{y_1}{g}\right] \qquad \text{(III.A.13)}$$

From the relation

$$\frac{\partial V}{\partial y} = B_y$$

$$V_o = B_o g$$

the total flux may be expressed

$$\varphi = B_o g \ell_{eff} \left[\frac{4}{\pi} \left(1 - \ell n \frac{4}{\pi} \right) + \frac{2b}{g} + \frac{4}{\pi} \ell n \frac{y_1}{g} \right] \qquad \text{(III.A.14)}$$

To calculate the flux density at any point in the field, use the relations

$$\frac{dW}{dz} = \frac{dW}{dt} \frac{dt}{dz} = \frac{\partial U}{\partial x} + j \frac{\partial V}{\partial y} \qquad \text{(III.A.15)}$$

and

$$\frac{\partial V}{\partial y} = \frac{\partial U}{\partial x} = \frac{V_o}{g} \text{ real } \left(\frac{t - a}{t + 1} \right)^{\frac{1}{2}} \qquad \text{(III.A.16)}$$

with $\frac{V_o}{g} = B_o$ as the flux density well inside the gap. Using Eq. (III.A.4) and considering that $h \gg g$, it is seen that

$$x + jy = \frac{g}{\pi} \ell n \left[\frac{\left(1 + \frac{1}{t} \right)^{\frac{1}{2}} + 1}{\left(1 + \frac{1}{t} \right)^{\frac{1}{2}} - 1} \right] - \frac{2}{\pi} g \left(1 + \frac{1}{t} \right)^{\frac{1}{2}} \qquad \text{(III.A.17)}$$

For $\frac{1}{t} \ll 1$,

$$x + \frac{2}{\pi} g = \frac{g}{\pi} \ell n (4t + 1)$$

or

$$t = \frac{1}{4} \left[e^2 \cdot e^{\pi x/g} - 1 \right] \qquad \text{(III.A.18)}$$

With Eq. (III.A.16), and remembering that $g \ll h$, this yields

$$B_y = \frac{\partial V}{\partial y} = B_o \left[\frac{e^2 \cdot e^{\pi x/g} - 1}{e^2 \cdot e^{\pi x/g} + 1} \right]^{\frac{1}{2}}$$

or

$$B_y = B_o \left[1 - e^{-\left(2+\frac{\pi x}{g}\right)} \right] \qquad \text{(III.A.19)}$$

and

$$1 - \frac{B_y}{B_o} = e^{-2} \cdot e^{-\pi x/g}$$

Computing x from the symmetry axis of the gap and using the notations $2w$ for the pole width, one may write from Eq. (III.A.19)

$$1 - \frac{B_y}{B_o} = \frac{1}{2e^2} \left[e^{-\frac{\pi}{g}(w-x)} + e^{-\frac{\pi}{g}(w+x)} \right]$$

$$1 - \frac{B_y}{B_o} = \frac{\cosh(\pi x/g)}{e^2 \cdot e^{\pi w/g}} \qquad \text{(III.A.20)}$$

which is in agreement to the result calculated by Hedin.[2]

In Fig 7 the field homogeneity versus x is given for rectangular pole edges, assuming $h \gg g$ and no effect from the exciting coils.

B. Curved Pole Boundaries

In the previous section it was shown that the flux density is increasing toward the sharp-edged corners. In order to limit the maximum flux density in the pole edges, and subsequently to extend the gap area with maximum field homogeneity, and not increasing the gap width, the corners have to be rounded. The calculation of the field distribution around a rounded pole edge may be found by a modified Schwartz-Christoffel transformation. The curve shape cannot be found precisely, but a fairly good approximation can be obtained from the following procedure: In Fig. 8 the pole corner is curved. The curvature to fulfill the following

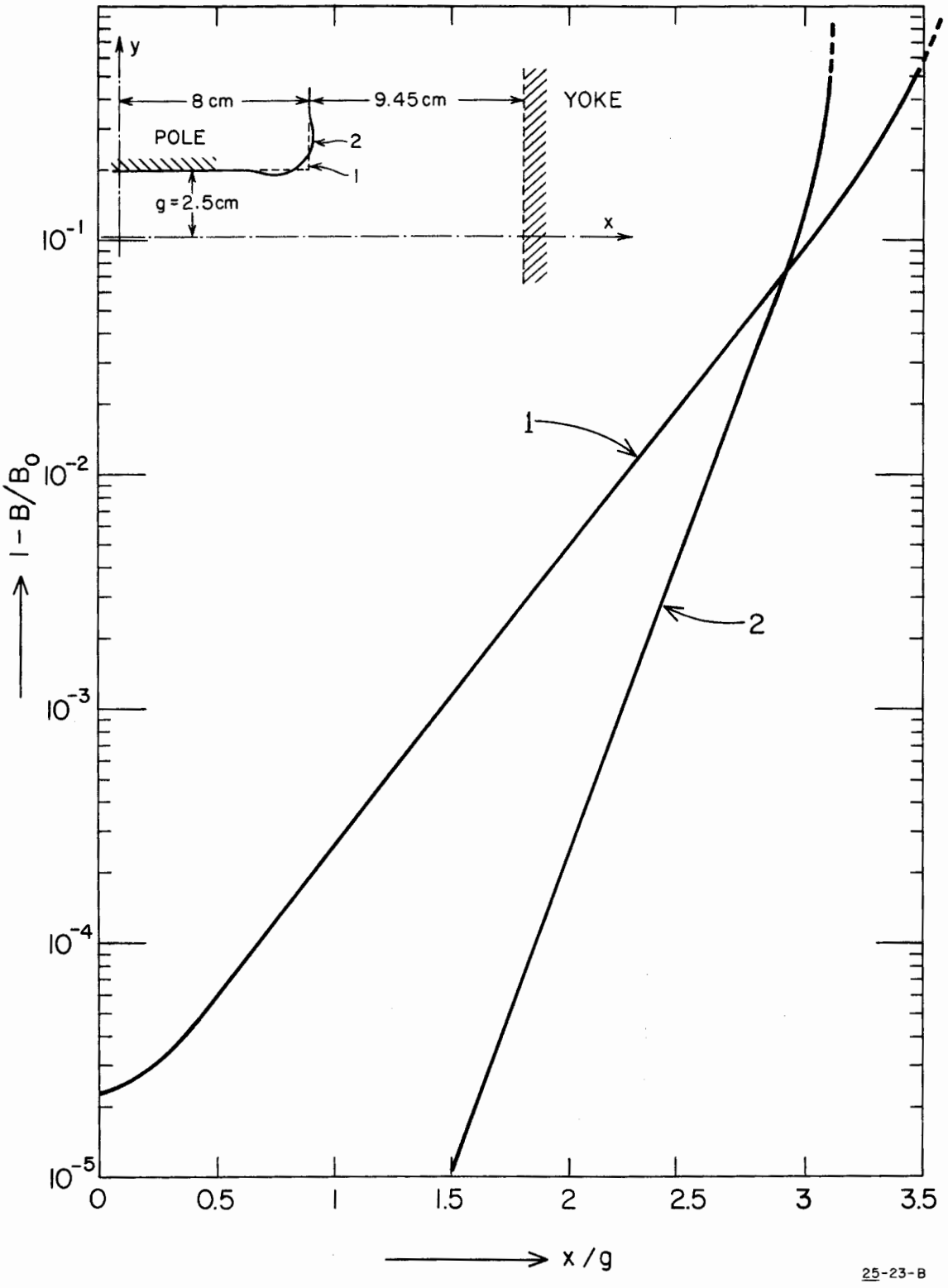

FIG. 7--Field distribution along the x axis in the gap.

1. Pole shape rectangular
2. Shimmed pole contour

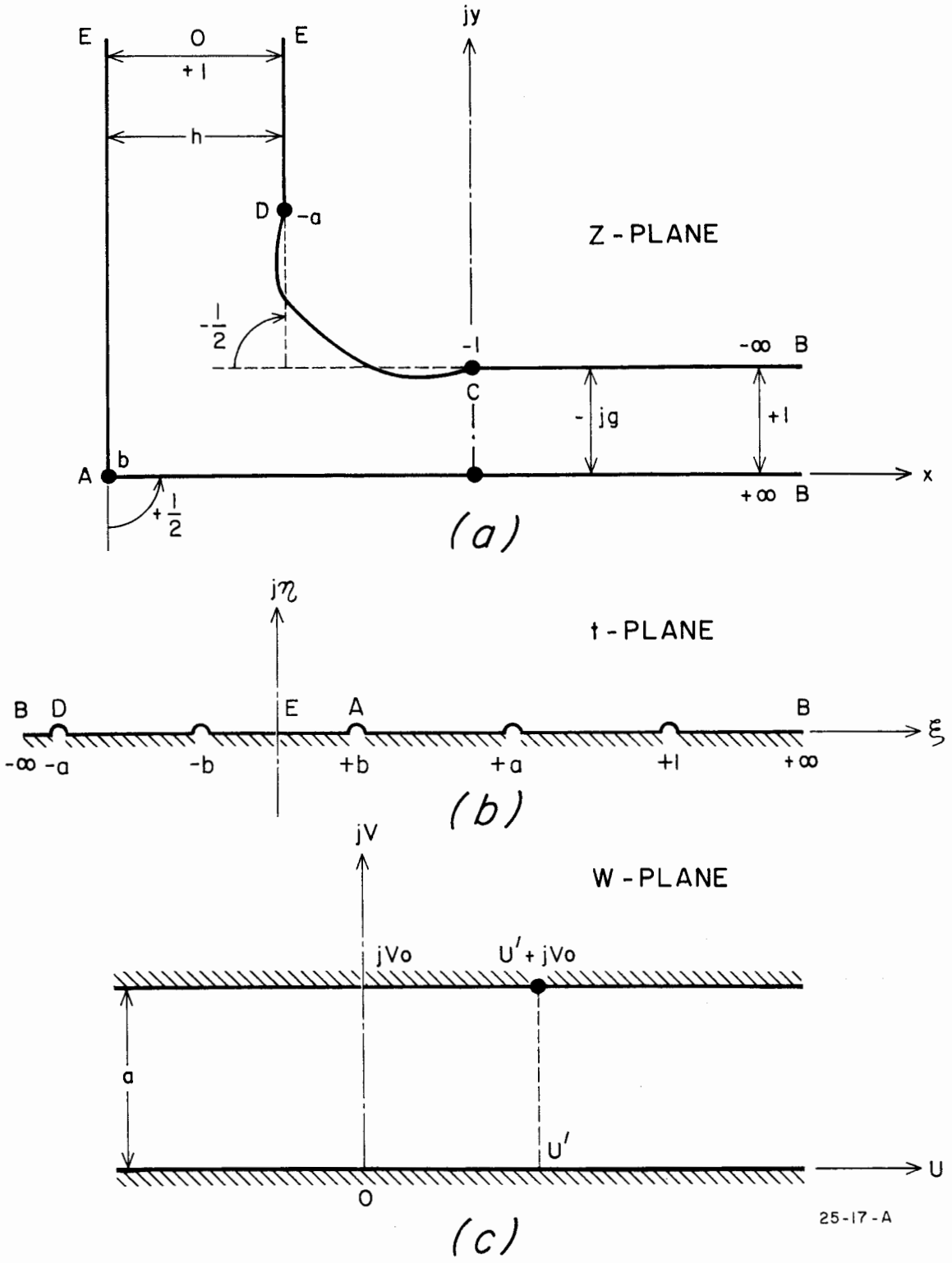

FIG. 8a, 8b, 8c--Pole and yoke configuration for calculation of field distribution along the gap.

requirements must be found:

a. For a given pole width the field homogeneity region inside the gap shall be a maximum.

b. The flux density ratio over the corner from the flat to the shimmed part of the pole face inside the gap should not exceed a certain preset value.

These two conditions, and the fact that the ratio h/g for a certain magnet is known, determine the pole curvature in a unique way. There is an optimum solution fulfilling the requirements. In the following, an outline of the procedure is given.

We proceed in the same way as in Section III.A and transform the real axis of the t-plane into the z-plane. The corresponding points of the two planes are:

C:	$z = jg$	$t = -1$
D:	$z = -x_1 + jy_1$	$t = -a$
E:	$z = -x_1 + jy_2$	$t = 0$
A:	$z = -x_2$	$t = +b$
B:	$z = +\infty$	$t = \infty$

The rounding of the pole face is achieved by introducing a factor λ,[3] which has to be determined such to fulfill certain required conditions mentioned above:

$$z = C_1 \int \frac{(1-\lambda)(t+a)^{\frac{1}{2}} + \lambda(t+1)^{\frac{1}{2}}}{t(t-b)^{\frac{1}{2}}}\, dt + C_2 \qquad \text{(III.B.1)}$$

The potential function (Fig. 8c) is

$$W = U + jV = \frac{V_o}{\pi} \int \frac{dt}{t} = \frac{V_o}{\pi} \ln t \qquad \text{(III.B.2)}$$

The combination of Eqs. (III.B.1) and (III.B.2) gives the required flux density:

$$\frac{dW}{dz} = \frac{1}{C_1} \cdot \frac{V_o}{\pi} \cdot \frac{(t-b)^{\frac{1}{2}}}{(1-\lambda)(t+a)^{\frac{1}{2}} + \lambda(t+1)^{\frac{1}{2}}} \qquad \text{(III.B.3)}$$

For $t \to \infty$,

$$\left.\frac{dW}{dz}\right|_{t \to \infty} = \frac{1}{C_1} \frac{V_o}{\pi} = \frac{V_o}{g} \qquad \text{(III.B.4)}$$

which gives:

$$C_1 = \frac{g}{\pi} \qquad \text{(III.B.5)}$$

For $t = 0$,

$$\left.\frac{dW}{dz}\right|_{t = 0} = j \frac{V_o}{g} \frac{(b)^{\frac{1}{2}}}{(1-\lambda)a^{\frac{1}{2}} + \lambda} = j \cdot \frac{V_o}{h} \qquad \text{(III.B.6)}$$

$$g/h = \frac{(b)^{\frac{1}{2}}}{(1-\lambda) \cdot a^{\frac{1}{2}} + \lambda} \equiv k_1 \qquad \text{(III.B.7)}$$

For $t = -1$,

$$\left.\frac{dW}{dz}\right|_{t = -1} = \frac{V_o}{g} \frac{(1+b)^{\frac{1}{2}}}{(1-\lambda)(1-a)^{\frac{1}{2}}} \qquad \text{(III.B.8)}$$

The following ratio is defined as:

$$k_2 = \left.\frac{dW}{dz}\right|_{t = -1} : \left.\frac{dW}{dz}\right|_{t = \infty} \qquad \text{(III.B.9)}$$

which gives:

$$k_2 = \frac{(1+b)^{\frac{1}{2}}}{(1-\lambda)(1-a)^{\frac{1}{2}}} \qquad \text{(III.B.10)}$$

For $t = -a$,

$$\left.\frac{dW}{dz}\right|_{t=-a} = j\,\frac{V_o}{g}\,\frac{(a+b)^{\frac{1}{2}}}{\lambda(1-a)^{\frac{1}{2}}} \qquad \text{(III.B.11)}$$

We define again the flux density ratio on the side face of the pole:

$$\left.\frac{dW}{dz}\right|_{t=-a} : \left.\frac{dW}{dz}\right|_{t=0} = k_3 \qquad \text{(III.B.12)}$$

or:

$$k_3 = \frac{1}{k_1} \cdot \frac{(a+b)^{\frac{1}{2}}}{\lambda(1-a)^{\frac{1}{2}}} \qquad \text{(III.B.13)}$$

Calculating λ from Eq. (III.B.7) and inserting in Eqs. (III.B.10) and (III.B.13), we get:

$$\lambda = \frac{(b)^{\frac{1}{2}} - k_1(a)^{\frac{1}{2}}}{k_1[1-a^{\frac{1}{2}}]} \qquad \text{(III.B.14)}$$

$$k_2 = k_1\left(\frac{1+b}{1-a}\right)^{\frac{1}{2}} \cdot \frac{1-a^{\frac{1}{2}}}{k_1 - b^{\frac{1}{2}}} \qquad \text{(III.B.15)}$$

$$k_3 = \left(\frac{a+b}{1-a}\right)^{\frac{1}{2}} \cdot \frac{1-a^{\frac{1}{2}}}{b^{\frac{1}{2}} - k_1 \cdot a^{\frac{1}{2}}} \qquad \text{(III.B.16)}$$

Choosing definite values for k_2 and k_3, we calculate a and b and finally λ for a given magnet. Figures 8d and 8e show the parameters a and b as a function of k_2 for various numbers of k_3, assuming $k_3 = \frac{1}{k_1}$.

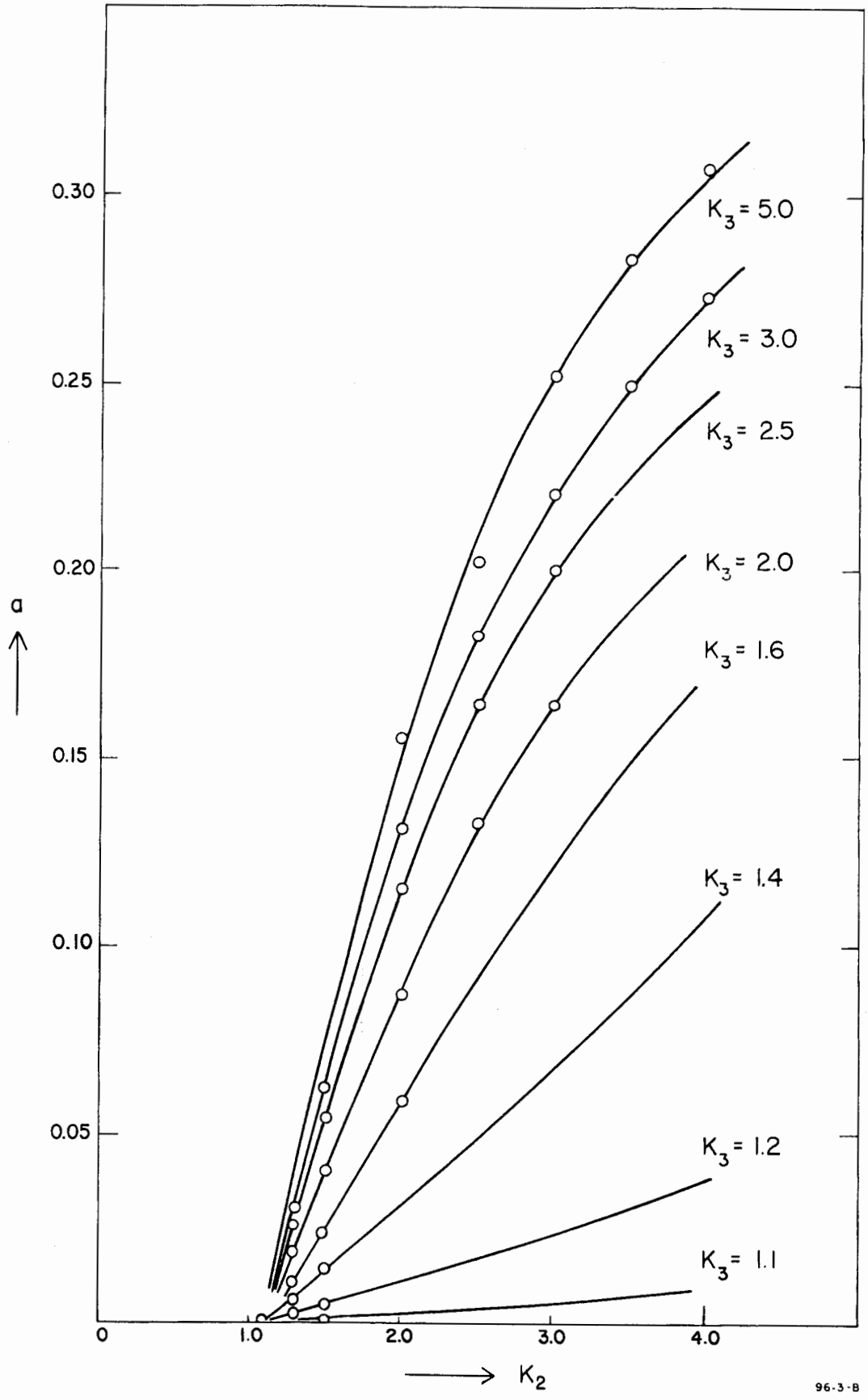
0.30
0.25
0.20
0.15
0.10
0.05
a
0
1.0
2.0
3.0
4.0
K2
K3 = 5.0
K3 = 3.0
K3 = 2.5
K3 = 2.0
K3 = 1.6
K3 = 1.4
K3 = 1.2
K3 = 1.1
96-3-B

Figure 8d

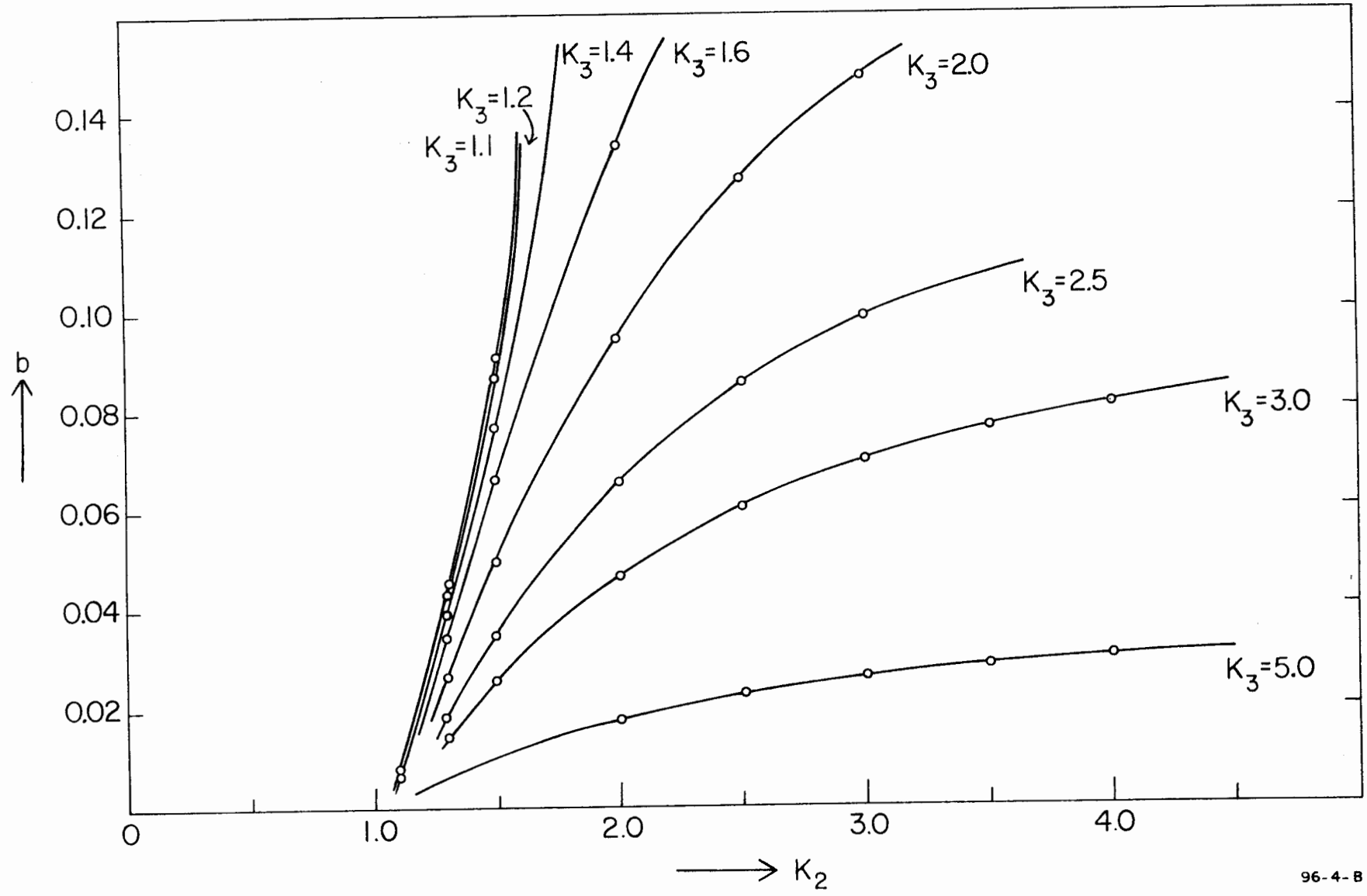
K_3=1.4
K_3=1.6
K_3=2.0
K_3=1.2
K_3=1.1
K_3=2.5
K_3=3.0
K_3=5.0
0.14
0.12
0.10
0.08
0.06
0.04
0.02
b
0
1.0
2.0
3.0
4.0
K_2
96-4-8

Figure 8e

$\lambda = 0$ represents a rectangular pole corner at $t = -a$.

$\lambda = 1$, $k_2 = \infty$ represents the rectangular pole corner at $t = -1$.

Both cases may be treated as shown in (III.A). For $1 > \lambda > 0$, the pole face in the region $-a < t < -1$ is shaped as shown in Fig. 8f. The figure shows the field distribution for the specific case of:

$$k_1 = \frac{g}{h} = 0.246 \qquad k_2 = 2.1 \qquad \text{and} \qquad k_3 = 2.35$$

which leads to

$$a = 0.1 \qquad b = 2.621 \cdot 10^{-2} \qquad \lambda = 0.5.$$

For $1 < \lambda < 0$ the pole face in the region $-a < t < -1$ is shaped as shown in Fig. 8g, the relations

$$k_1 = 0.246 \qquad k_2 = -0.95 \qquad k_3 = 10$$

lead to

$$a = 0.2 \qquad b = 6.9 \cdot 10^{-3} \qquad \lambda = -0.2.$$

All cases of $\lambda < 0$ give circular shaped pole faces in the region $-a < t < -1$.

For our particular magnet the pole face is according to the dotted equipotential line with the ratio $k_1 = \frac{g}{h} = 0.246$ maintained.

The flux density at any point in the gap may be calculated from the relation:

$$\frac{dV}{dy} = \frac{dU}{dx} = \frac{V_o}{g} \cdot \text{real} \frac{(t - b)^{\frac{1}{2}}}{(1 - \lambda)(t + a)^{\frac{1}{2}} + \lambda(t + 1)^{\frac{1}{2}}} \qquad \text{(III.B.17)}$$

For our particular case the value of

$$1 - \frac{B_y}{B_o} = f(x)$$

is calculated and shown in Fig. 7.

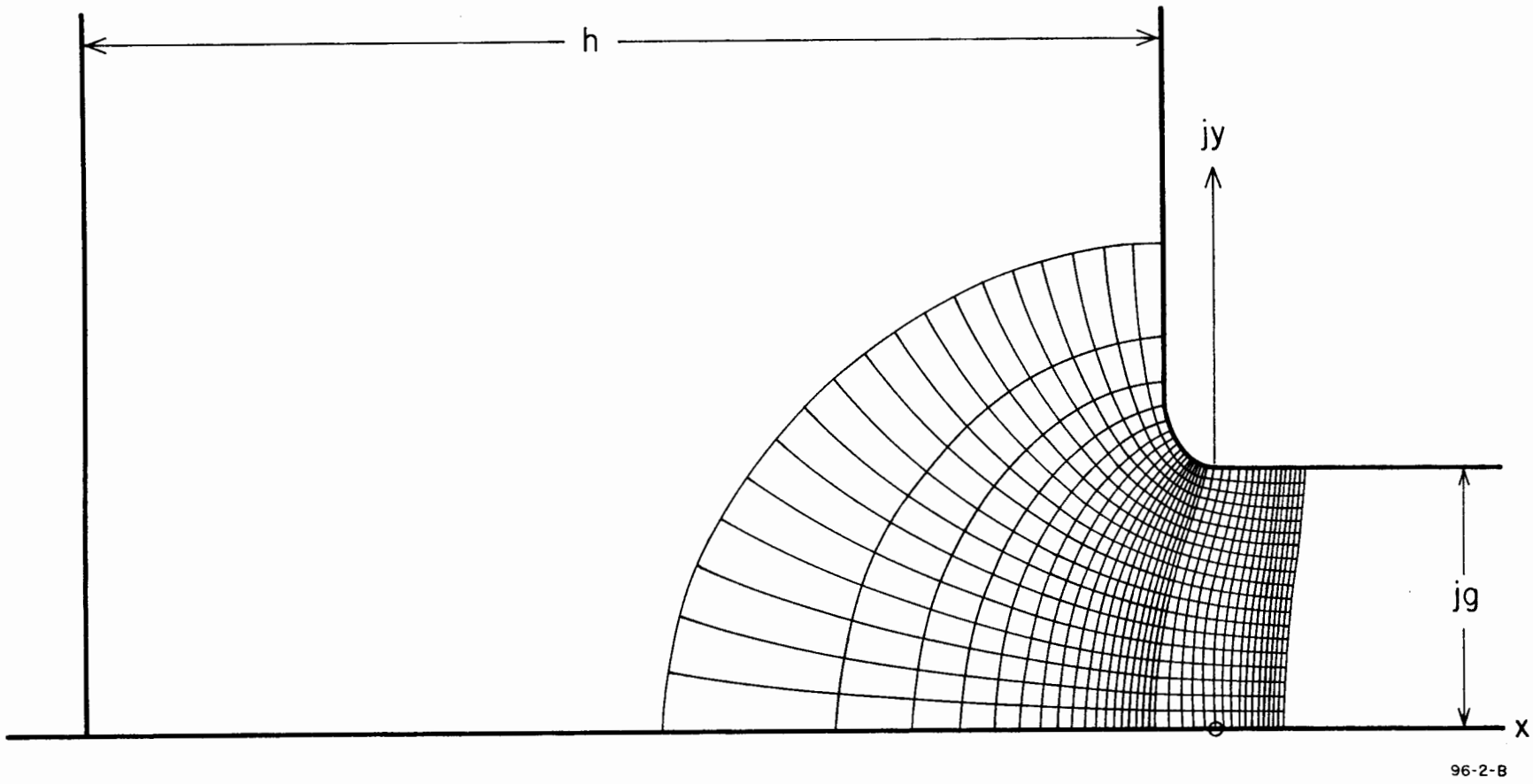

Figure 8f

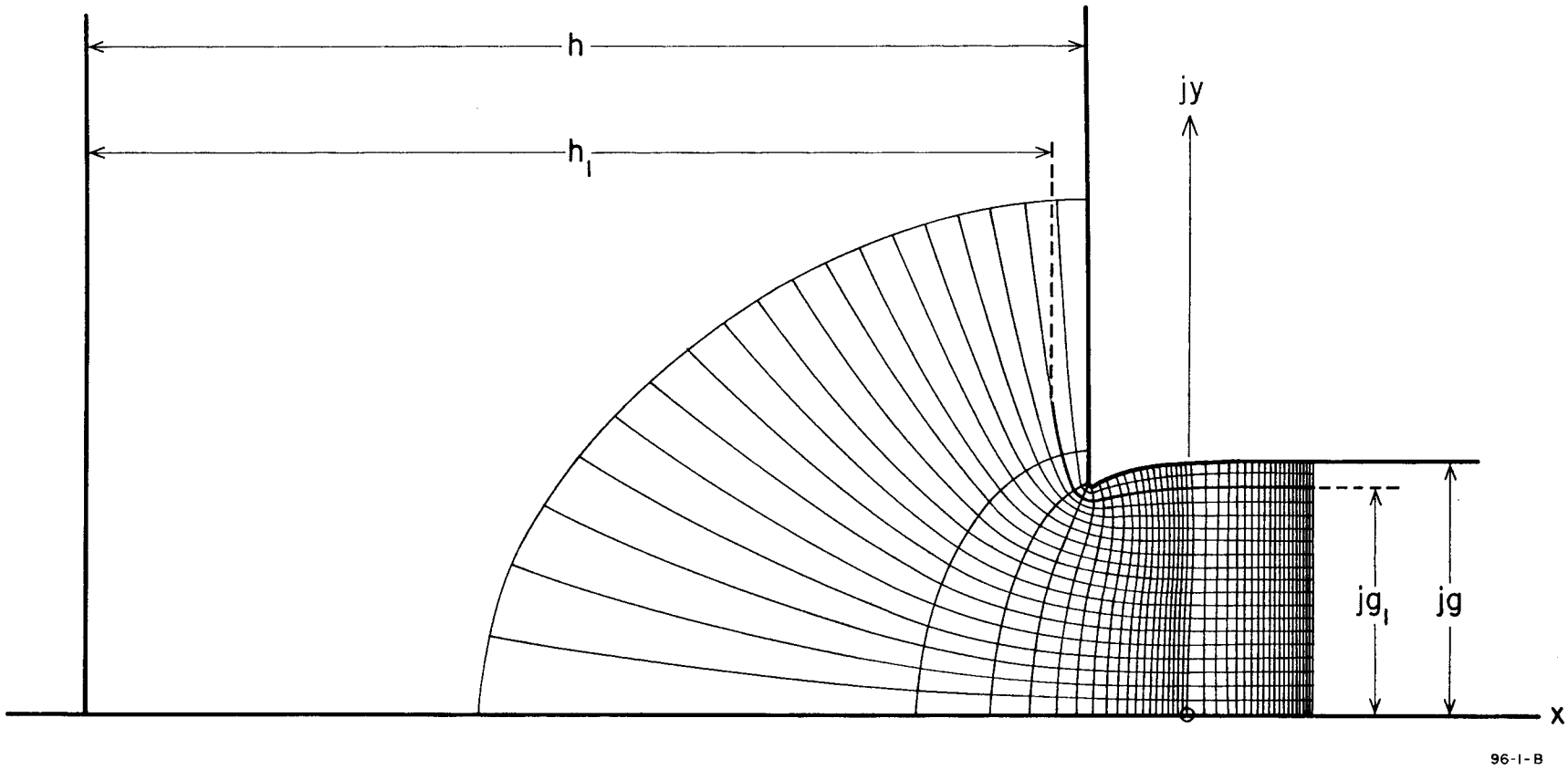

Figure 8g

To integrate Eq. (III.B.1) use the substitution:

$$u_1 = \left(\frac{t + a}{t - b}\right)^{\frac{1}{2}} \quad \text{and} \quad u_2 = \left(\frac{t + 1}{t - b}\right)^{\frac{1}{2}}$$

and obtain

$$z = \frac{g}{\pi}(1 - \lambda)\left\{\ln \frac{\left(\frac{t + a}{t - b}\right)^{\frac{1}{2}} + 1}{\left(\frac{t + a}{t - b}\right)^{\frac{1}{2}} - 1} - 2\left(\frac{a}{b}\right)^{\frac{1}{2}} \cdot \tan^{-1}\left(\frac{b}{a} \cdot \frac{t + a}{t - b}\right)^{\frac{1}{2}}\right\}$$

$$+ \frac{g}{\pi}\lambda\left\{\ln \frac{\left(\frac{t + 1}{t - b}\right)^{\frac{1}{2}} + 1}{\left(\frac{t + 1}{t - b}\right)^{\frac{1}{2}} - 1} - 2\left(\frac{1}{b}\right)^{\frac{1}{2}} \cdot \tan^{-1}\left(b \cdot \frac{t + 1}{t - b}\right)^{\frac{1}{2}}\right\} + C_2 . \qquad \text{(III.B.18)}$$

At $t = -1$, $z = jg$ we have

$$C_2 = -\frac{g}{\pi}(1 - \lambda)\left\{\ln \frac{1 + \left(\frac{1 - a}{1 + b}\right)^{\frac{1}{2}}}{1 - \left(\frac{1 - a}{1 + b}\right)^{\frac{1}{2}}} - 2\left(\frac{a}{b}\right) \cdot \tan^{-1}\left(\frac{b}{a} \cdot \frac{1 - a}{1 + b}\right)^{\frac{1}{2}}\right\}$$

For $h \gg g$ (true for most magnets), we have $b \ll a < 1$, and may write

$$z = \frac{g}{\pi}(1 - \lambda)\left\{\ln \frac{\left(1 + \frac{a}{t}\right)^{\frac{1}{2}} + 1}{\left(1 + \frac{a}{t}\right)^{\frac{1}{2}} - 1} - 2\left(\frac{a}{b}\right)^{\frac{1}{2}} \cdot \tan^{-1}\left[\frac{b}{a} \cdot \left(1 + \frac{a}{t}\right)\right]^{\frac{1}{2}}\right.$$

$$\left. - \ln \frac{1 + (1 - a)^{\frac{1}{2}}}{1 - (1 - a)^{\frac{1}{2}}} + 2\left(\frac{a}{b}\right)^{\frac{1}{2}} \cdot \tan^{-1}\left[\frac{b}{a}(1 - a)\right]^{\frac{1}{2}}\right\}$$

$$+ \frac{g}{\pi}\lambda\left\{\ln \frac{\left(1 + \frac{1}{t}\right)^{\frac{1}{2}} + 1}{\left(1 + \frac{1}{t}\right)^{\frac{1}{2}} - 1} - \frac{2}{(b)^{\frac{1}{2}}} \cdot \tan^{-1}\left[b\left(1 + \frac{1}{t}\right)\right]^{\frac{1}{2}}\right\} \qquad \text{(III.B.19)}$$

For $-a < t < 0$,

$$z = jg + \frac{g}{\pi}(1-\lambda)\left[\ln\frac{1+j(-1-\frac{a}{t})^{\frac{1}{2}}}{1-j(-1-\frac{a}{t})^{\frac{1}{2}}} - 2j(-1-\frac{a}{t})^{\frac{1}{2}} - \ln\frac{1+(1-a)^{\frac{1}{2}}}{1-(1-a)^{\frac{1}{2}}} + 2(1-a)^{\frac{1}{2}}\right]$$

$$+ \frac{g}{\pi}\lambda\left[\ln\frac{1+j(-1-\frac{1}{t})^{\frac{1}{2}}}{1-j(-1-\frac{1}{t})^{\frac{1}{2}}} - 2j(-1-\frac{1}{t})^{\frac{1}{2}}\right] \qquad \text{(III.B.20)}$$

At E with $x = -x_1$ and $y = y_2 \gg g$, $t \to 0$ and:

$$y_2 = g + \frac{2g}{\pi}(1-\lambda)\left[\tan^{-1}(-1-\frac{a}{t})^{\frac{1}{2}} - (-1-\frac{a}{t})^{\frac{1}{2}}\right] + \frac{2g}{\pi}\lambda\left[\tan^{-1}(-1-\frac{1}{t})^{\frac{1}{2}} - (-1-\frac{1}{t})^{\frac{1}{2}}\right]$$

(III.B.21)

or

$$y_2 = -\frac{2g}{\pi}\left[(1-\lambda)(-\frac{a}{t})^{\frac{1}{2}} + \lambda(-\frac{1}{t})^{\frac{1}{2}}\right] \qquad \text{(III.B.22)}$$

and

$$t = -\left(\frac{2g}{\pi y_2}\right)^2\left[(1-\lambda)(a)^{\frac{1}{2}} + \lambda\right]^2 . \qquad \text{(III.B.23)}$$

Combining Eq. (III.B.23) with Eq. (III.B.2) we get:

$$. U_1 = \frac{2V_o}{\pi} \cdot \ln\left\{\left(\frac{2g}{\pi y_2}\right)\left[(1-\lambda)(a)^{\frac{1}{2}} + \lambda\right]\right\} \qquad \text{(III.B.24)}$$

For the region $-\infty < t < -a$ we have:

$$z = jg + \frac{g}{\pi}(1-\lambda)\left[\ln\frac{1+(1+\frac{a}{t})^{\frac{1}{2}}}{1-(1+\frac{a}{t})^{\frac{1}{2}}} - 2(1+\frac{a}{t})^{\frac{1}{2}} - \ln\frac{1+(1-a)^{\frac{1}{2}}}{1-(1-a)^{\frac{1}{2}}} + 2(1-a)^{\frac{1}{2}}\right]$$

$$+\frac{g}{\pi}\left[\ln\frac{1+(1+\frac{1}{t})^{\frac{1}{2}}}{1-(1+\frac{1}{t})^{\frac{1}{2}}} - 2(1+\frac{1}{t})^{\frac{1}{2}}\right] \qquad \text{(III.B.25)}$$

For a point:

$$y = y_3 = jg \qquad x = x_3 \gg g$$

we get for $t \to -\infty$

$$x_3 = \frac{g}{\pi}(1-\lambda)\left[2\cdot\ln 2 + \ln t - 2 - \ln\frac{1+(1-a)^{\frac{1}{2}}}{1-(1-a)^{\frac{1}{2}}} + 2(1-a)^{\frac{1}{2}}\right]$$

$$+\frac{g}{\pi}\lambda\left[2\cdot\ln 2 + \ln t - 2\right] \qquad \text{(III.B.26)}$$

or

$$\ln t = 2 - 2\ln 2 + (1-\lambda)\left[\ln\frac{1+(1-a)^{\frac{1}{2}}}{1-(1-a)^{\frac{1}{2}}} - 2(1-a)^{\frac{1}{2}}\right] + \frac{\pi x_3}{g} \qquad \text{(III.B.27)}$$

and

$$U_2 = \frac{V_o}{\pi}\left\{2 - 2\ln 2 + (1-\lambda)\left[\ln\frac{1+(1-a)^{\frac{1}{2}}}{1-(1-a)^{\frac{1}{2}}} - 2(1-a)^{\frac{1}{2}}\right] + \frac{\pi x_3}{g}\right\} \qquad \text{(III.B.28)}$$

From (III.B.24) and (III.B.28) the flux per unit length is calculated:

$$U_2 - U_1 = V_o\left\{\frac{2}{\pi} - \frac{2}{\pi}\ln\frac{4}{\pi} + (1-\lambda)\left[\ln\frac{1+(1-a)^{\frac{1}{2}}}{1-(1-a)^{\frac{1}{2}}} - 2(1-a)^{\frac{1}{2}}\right] + \frac{x_3}{g}\right.$$

$$\left. + \frac{2}{\pi}\ln\frac{y_2}{g} - \frac{2}{\pi}\ln\left[(1-\lambda)(a)^{\frac{1}{2}} + \lambda\right]\right\}. \qquad \text{(III.B.29)}$$

In (III.B.29) $V_o\frac{x_3}{g}$ represents the homogenous part of the flux inside the gap.

$\frac{2V_o}{\pi}\ln\frac{y_2}{g}$ represents the flux between the sides of the pole perpendicular to the gap and

$$V_o\left[\frac{2}{\pi} - \frac{2}{\pi}\ln\frac{4}{\pi} + (1-\lambda)\left[\ln\frac{1+(1-a)^{\frac{1}{2}}}{1-(1-a)^{\frac{1}{2}}} - 2(1-a)^{\frac{1}{2}}\right] - \frac{2}{\pi}\ln\left[(1-\lambda)(a)^{\frac{1}{2}} + \lambda\right]\right]$$

is the additional flux due to the shape of the pole edges. The total flux which enters the pole face is:

$$\Phi = B_o \cdot g \cdot \ell_{eff}\left\{\frac{4}{\pi}\left(1 - \ln\frac{4}{\pi} - \ln\left[(1-\lambda)(a)^{\frac{1}{2}} + \lambda\right]\right) + \frac{2x_3}{g}\right.$$

$$\left. + \frac{4}{\pi}\ln\frac{y_2}{g} + 2(1-\lambda)\left[\ln\frac{1+(1-a)^{\frac{1}{2}}}{1-(1-a)^{\frac{1}{2}}} - 2(1-a)^{\frac{1}{2}}\right]\right\} \qquad \text{(III.B.30)}$$

C. Pole End Effects

In calculating the end effect of a finite pole length, it is customary to assume that the magnetic field is constant to a virtual field boundary

located at a distance ℓ from the pole edge. The distance ℓ is chosen according to experience for rectangular-shaped pole ends to be 0.5 to 1 air gap. The length of this field with constant amplitude B_o is called ℓ_{eff} of the magnet (Fig. 9a).

If the magnet is provided with mirrors on both ends, rectangular pole edges may be calculated according to Eq. (III.A.20) for $g/h' \ll 1$ (h' is the distance between pole face and mirror) as

$$1 - \frac{B_{y_o}}{B_o} = \frac{1}{e^2} e^{-\pi \ell/g} \cosh(\pi z/g) \qquad \text{(III.C.1)}$$

Off the median plane the field components may be expressed in the form of a Taylor series in y, the distance from the meridian plane. The field is symmetric with respect to the plane $y = 0$, and by neglecting the higher terms the second order may be expressed as

$$B_y = B_{y_o} + \frac{y^2}{2!}\left(\frac{\partial^2 B_y}{\partial y^2}\right)_{y=o} \qquad \text{(III.C.2)}$$

B_{y_o} is the field of the fringing field at $y = 0$.

Equation (III.C.2) requires the knowledge of B_{y_o} given in Eq. (III.C.1). The effective length of the magnet can be determined with sufficient accuracy when the pole ends of the magnet are shaped accordingly and fringing field-correcting magnetic shields (in the following called mirrors) are placed axially in both magnet ends. One possible solution, which makes the effective length of the magnetic field in the meridian plane of the gap independent of the exciting current, and therefore of the field amplitude, is to form the pole ends so that the fringing field follows a quadrupole pattern. The field gradient in the z-y plane becomes constant. The field pattern is shown in Fig. 9b. As is shown in a paper by Brechna and Hedin,[4] the pole ends have to obey the equation:

$$zy^2 = \frac{g^3}{2 \tan \alpha} \qquad \text{(III.C.3)}$$

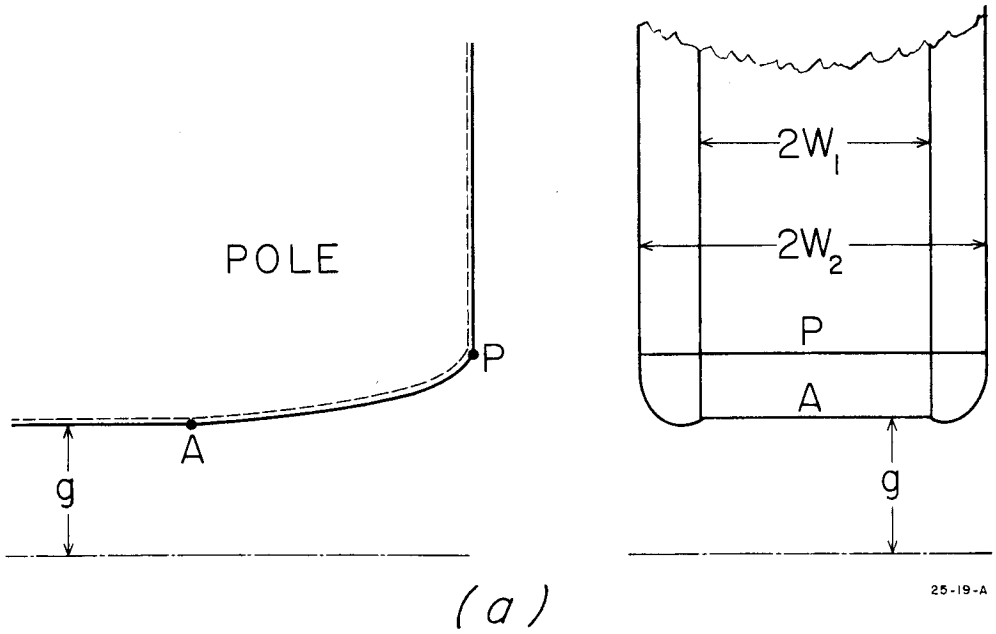

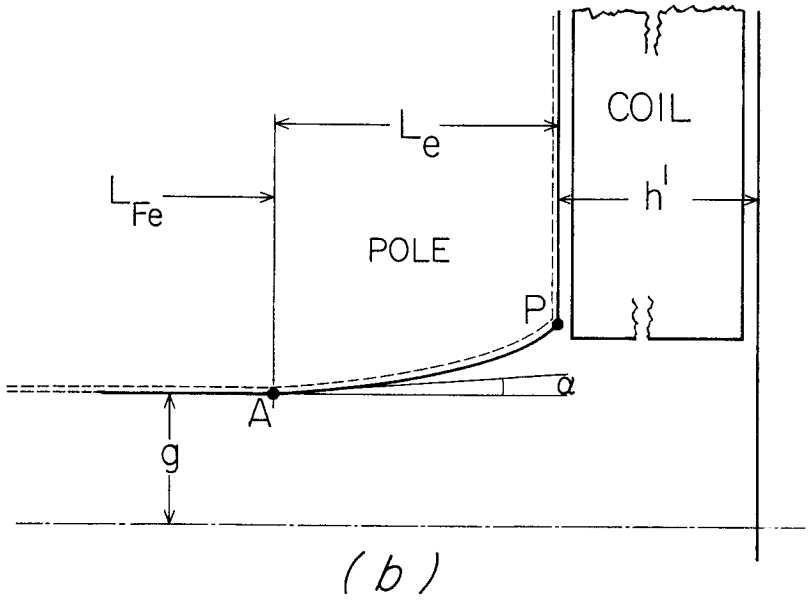

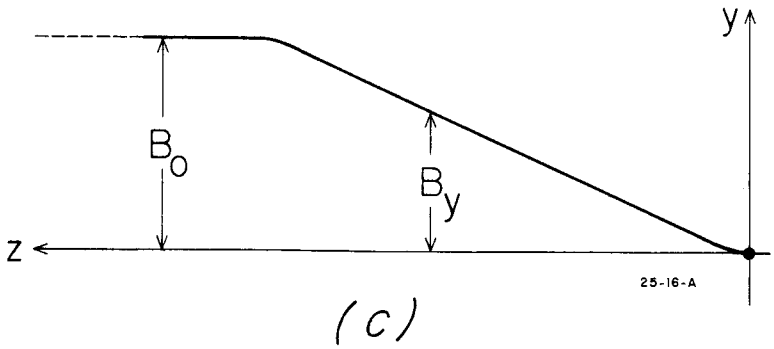

FIG. 9--Pole end shaping and field distribution.

The α can be determined from the radial position of the exciting coil with respect to the pole edge. The pole corner P should preferably be hidden behind the coil. The distance between pole face and mirrors is determined by the coil width. It is possible to choose α such that only a small perturbance in the transition area between the homogeneous and the quadrupole field is present. Normally an angle of $\alpha = 4 \ldots 10^{\circ}$ has proved to be adequate.

IV. DESIGN PARAMETERS

A. The Exciting Coils

As mentioned in Section I, the magnet is pulsed with a frequency of $f = 1000\ \text{sec}^{-1}$. The current flowing through the coil during each pulse has the shape of a half sine wave. The pulse repetition rate is 360 pps. The pulse pattern may be chosen in such a way that many successive pulses of positive or negative polarity may energize the magnet. However, for the design of the coil, this choice is random. The current pattern shown in Fig. 4c is a succession of half sine waves with an average current of

$$I_{av} = \frac{2I_p}{\pi}\left(\frac{d}{T}\right) \qquad \text{(IV.A.1)}$$

and an rms value of

$$I_{rms} = I_p\left(\frac{d}{2T}\right)^{\frac{1}{2}} \qquad \text{(IV.A.2)}$$

which gives, for $f = 1000\ \text{sec}^{-1}$ and a pulse repetition rate of 360 pps,

$$I_{av} = 36.3 \text{ amperes}$$

$$I_{rms} = 95 \text{ amperes}$$

The fringing field in the region of the coils causes eddy current losses in the conductors. The exact calculation of these losses during the pulse is somewhat difficult, due to the peculiar pattern of the field in the windows. The eddy current losses are calculated from the skin effect phenomena in the conductors, which are expressed by a higher resistance than the dc resistance of the coil. The ratio of the ac to dc losses,[5] suitably modified for the pulsed magnet, may be expressed as

$$\frac{R_{\sim}}{R_{=}} = H + \left[k + 0.25 \left(\frac{Kbm}{D} \right)^2 \left(\frac{d_o}{c} \right) \right] Gn^2 \left(\frac{d_s}{d_o} \right)^2 \qquad \text{(IV.A.3)}$$

H and G are functions of the conductor diameter, the electric conductivity of the material κ and the applied frequency f. H and G in terms of the function x are given in Fig. 10. The function x is expressed as

$$x = \pi d (2\pi f \cdot \kappa)^{\frac{1}{2}} \qquad \text{(IV.A.4)}$$

For small values of x, say $0 \leq x \leq 0.4$, the value of G is

$$G \approx \frac{x^4}{64} \qquad \text{(IV.A.5)}$$

The constant k is a function of the number of strands n in the conductor. For $n > 100$, $k = 2$. For $n \leq 20$, $k = 1.5 \ldots 1.9$.

The other values (such as K, b, m, etc.) are shown in Fig. 11, with d_s as the diameter of each individual strand and the d_o as the diameter of the bare conductor; c is in the spacing between the centers of adjacent turns.

In order to keep the resistance ratio near unity, the conductor used in the pulsed magnet is chosen as a multistranded cable. It has a core of soft copper tube with a 0.395-cm hydraulic diameter for water cooling and five layers of individually insulated strands wound around the copper

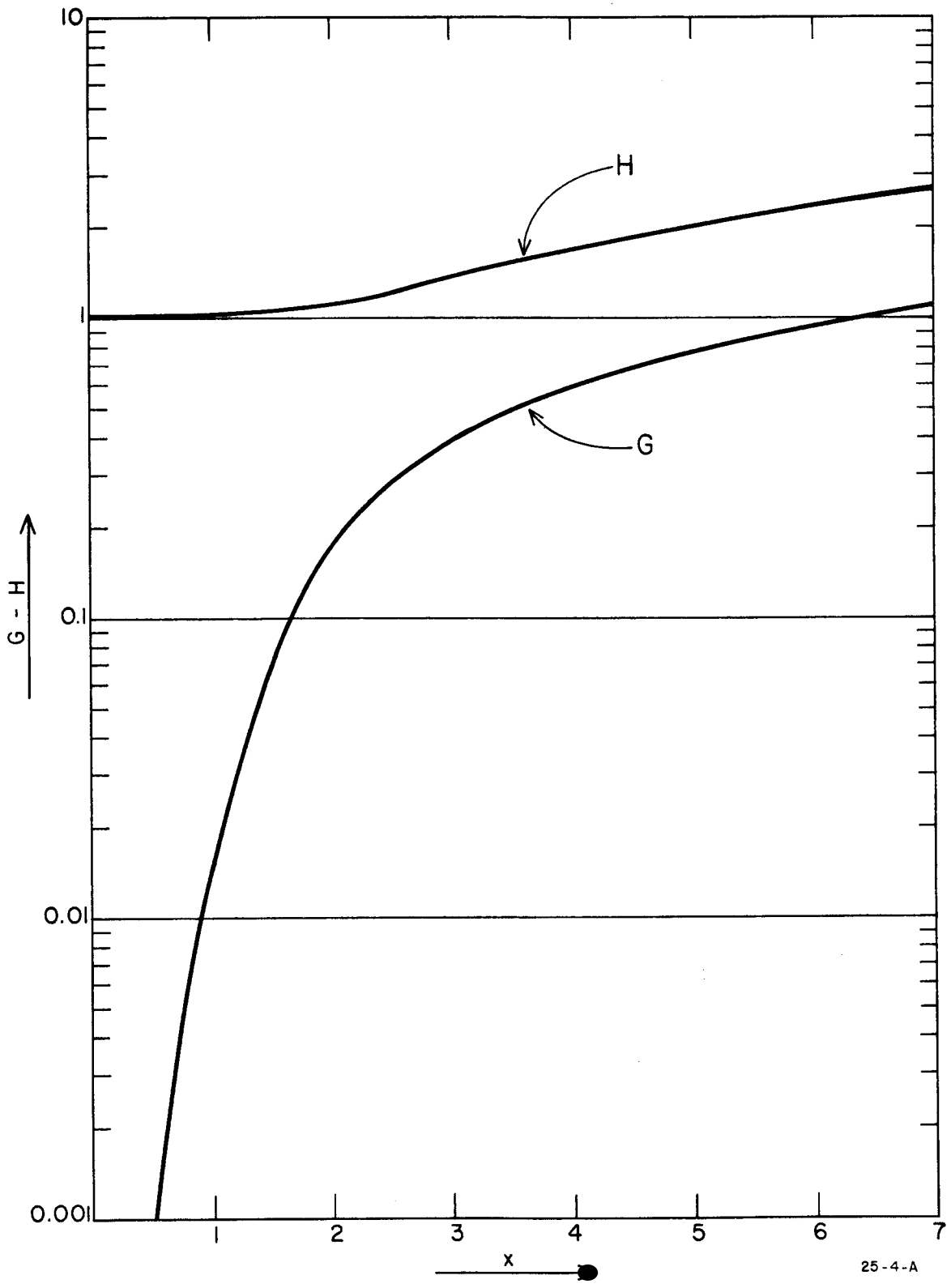

FIG. 10--Value of the function G and H to be used in connection with Equation (IV.A.3).

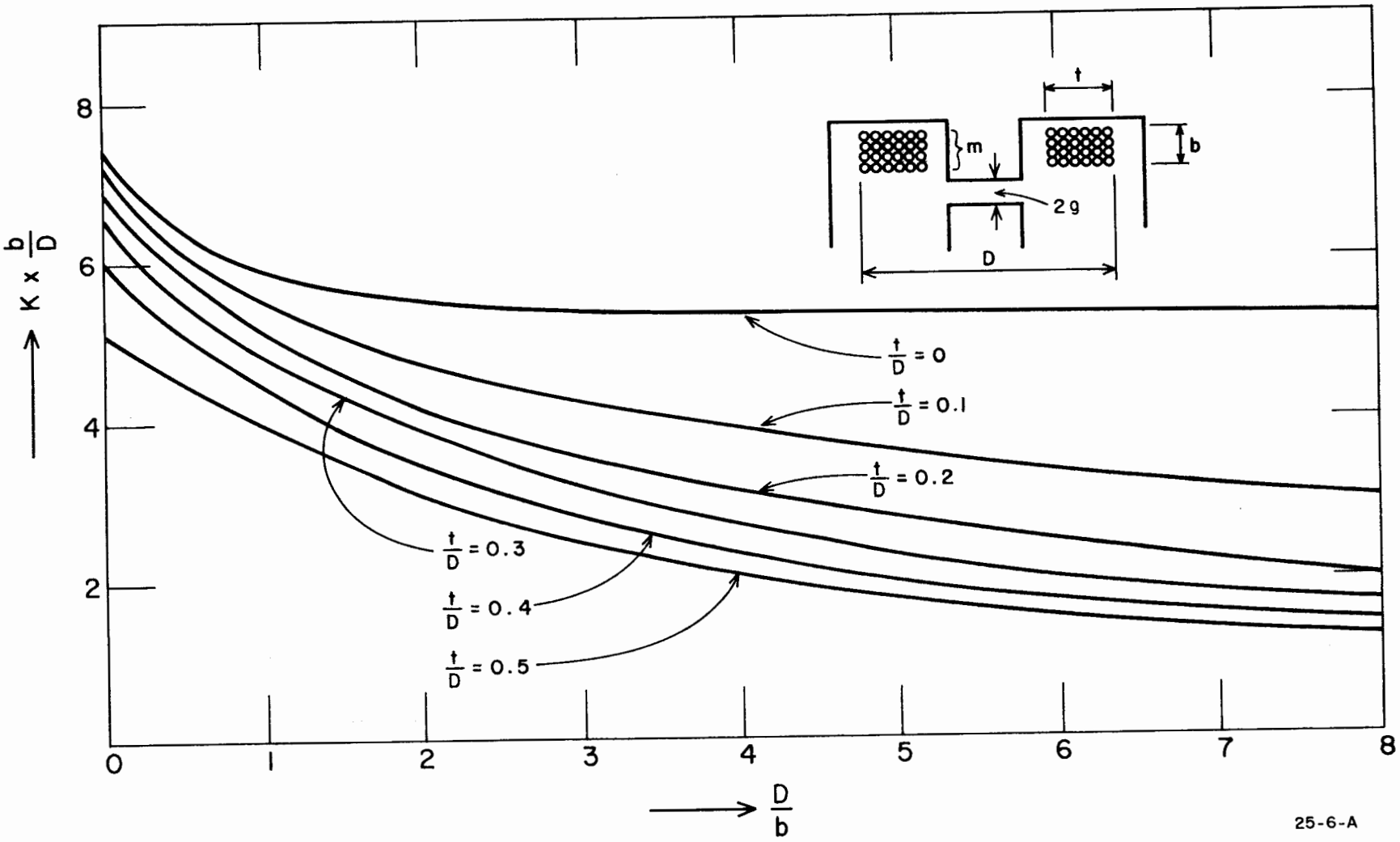

FIG. 11--Value of K to be used for calculation of ac resistance.

tube. The cable buildup is given in Table II. The cable is insulated with six layers of Volan A-treated fiberglass tape, giving an outer cable diameter of 1.6 cm. The effective copper cross section is 8.3×10^{-5} meters^2.

TABLE II

CONSTRUCTION OF CABLE

1st layer	24 strands	wire AWG No. 22
2nd layer	30 strands	wire AWG No. 22
3rd layer	30 strands	wire AWG No. 20
4th layer	36 strands	wire AWG No. 20
5th layer	34 strands	wire AWG No. 18

As shown in Table I and Section I, the number of turns per pole was chosen to be 24. The two coils with 24 turns may be connected in parallel, or two conductors per coil can be wound in parallel and the two poles connected in series. Each coil is insulated in three steps under a vacuum of $\leq$ 1 mm Hg. Around the coil, the ground insulation consists of an AIEE temperature class F or H epoxy with at least 50% (by weight of the total composite) fine mesh alumina filler. The coil impregnant is a low viscosity epoxy of AIEE-temperature class F or H. The casting and impregnation will be performed as follows.

1. The filled epoxy will be poured around the coil under vacuum. The top coil surface is not covered by epoxy.
2. The low viscosity epoxy will be poured on the coil under vacuum to impregnate the coil. The coil surface should be barely covered by epoxy.
3. The filled epoxy is then poured to cover the coil.

This technique guarantees that there would be no distinct difference in the transient area between impregnant and the casting around the coil. In order to prevent the filled epoxy around the coil from an early curing, before the impregnation and casting of the coil is completed, either epoxies with long pot life can be chosen, or the mold walls will

be kept cool until the curing process starts. The highly filled epoxy around the coil is important to insure high radiation properties of the coil structure; it has nearly the same thermal expansion coefficient as the conductor material. The filled epoxy penetrates only slightly between strands inside the cable insulation. Wrapping the coil with an open weave glass fiber has in this particular case many disadvantages and makes the impregnation of the coil exceedingly difficult.

The ratio of ac to dc resistance may be calculated from Eq. (IV.A.3) and Fig. 11 with $x = 0.35$, $H \approx 1$, and $G = 2.34 \times 10^{-4}$ as

$$\frac{R_{\sim}}{R_{=}} = 2.5$$

or

$$R_{\sim} = 2.5 \times R_{=} = 1.65 \times 10^{-2} \text{ ohms} \quad (\text{at } 60^{\circ}\text{C})$$

The total ohmic losses in the coil are, by Eq. (IV.A.2),

$$P_{\sim} = 150 \text{ watts}$$

The cooling water flows through the cooling tubes of both coils and then through the cooling channels that are welded to the core. In a first assumption the temperature rise of water passing through the coils was chosen to be 10°C. The temperature rise of the water cooling the core is calculated in Section IV.B.

B. The Magnet Core

The magnet core requires magnetic materials with the following characteristics. The flux directions inside the core lead to the choice of "non-oriented" silicon sheets, i.e., their magnetic properties with the direction of rolling are random. Cold reduced sheets are preferred over hot rolled sheets simply because of their superior surface condition. Of course, since the great proportion of mechanical

working of the sheets both in hot and cold conditions is in one direction, the "non-oriented" sheets with low loss factor per unit weight show some crystal directionality. Very often a proportion of 0.9:1 in loss ratio is found between the rolling direction and that perpendicular to it. However, the effect upon the magnetic properties measured in the directions of rolling to a direction perpendicular to it are insignificant or may be taken into consideration in the design. Even if the flux density in the gap is chosen to be low (as in our case), some part of the core may be saturated. The saturation effect in the iron corners (which leads to a reduction of the iron length in the slimmer pole parts) upon the calculation of iron ampere-turns may be taken into account from the simple relation

$$[B(z)s]_{out} = \int \frac{B_{in}}{\mu(B)} dr \qquad \text{(IV.B.1)}$$

The high pulse frequency of $f = 10^3$ sec^{-1} dictates the choice of thin transformer sheets. A compromise to select the best qualified sheets, used normally in transformers for a low cost, was made in the choice of 0.35-mm silicon sheets with a loss factor of ≈ 3.75 watts/kg (1.7 watts/lb) at 0.2 weber/meter^2 and 10^3 cps frequency (12a).

Loss factors of "non-oriented" sheets are not specifically affected by cutting and punching individual sheets, but stress-relieving annealing of sheets has been specified after the cutting of the sheets to reduce strain and improve magnetic properties.

Local strains, which may be caused from non-uniform pressing of the stacks, lead to an increase of the loss factor.[6] To avoid local strain buildup, the core is pressed by means of a hydraulic press under 3 kg/cm^2 after very careful stacking and then is welded on the outside surfaces. At this pressure the interlamination resistance was measured to be 300 ohms/cm^2/sheet. Local heating during the welding must be avoided to eliminate additional strains in the sheets.

The sheets are covered on both surfaces with a high temperature insulation with a maximum thickness of 0.025 mm (fill factor ≈ 0.9). The sheets must be carefully deburred after cutting and punching and placed on a smooth surface to avoid deviation from a plane surface. Another

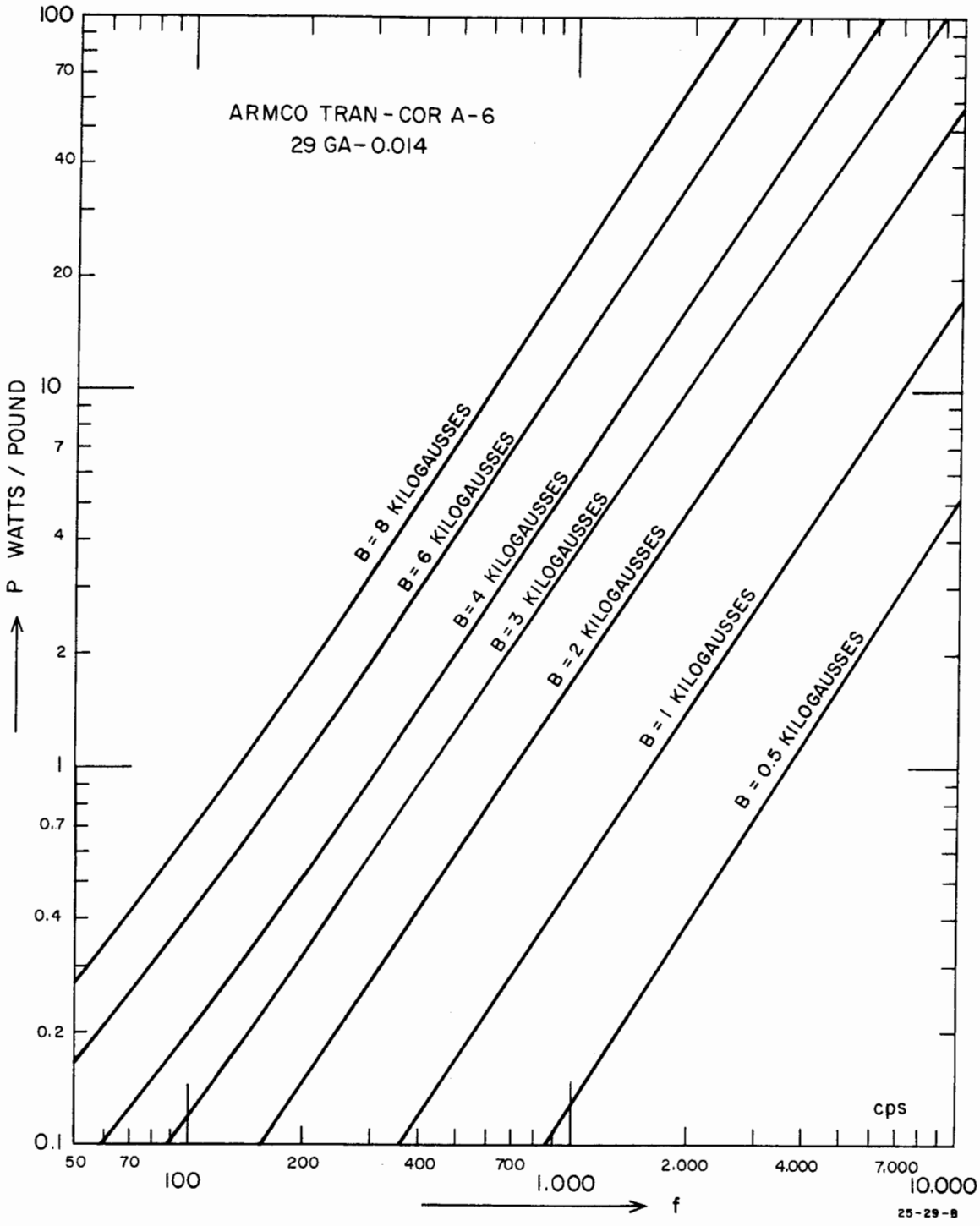

FIG. 12a--Core losses at higher frequencies.

important feature of the magnet is the required low remanent field in the gap. Nickel-iron sheets were not selected, mainly because of their high cost and grain orientation. Instead, the flux density was chosen to be moderate, both to eliminate excessive magnetostrictive forces in the core and to reduce the remanent flux density to about 1.2×10^{-4} weber/meter^2 in the gap (see Fig. 12b and Fig. 2). The magnetization curves of the silicon sheets to be used in the magnet are shown in Fig. 12c.

After the welding of U-shape frames and cooling tubes on the outer surfaces of the core, the core is impregnated under vacuum in a low viscosity AIEE temperature class H epoxy.

The weight of the yokes is 1410 kg and the peak value of the iron losses is 3105 watts. The weight of the poles is 220 kg with a peak loss value of 955 watts in nominal operation.

Assuming 30% additional core losses due to the cutting, stamping, and pressing of the sheets, the loss peak value of the core is

$$P_{peak} = 5300 \text{ watts}$$

The average losses, therefore, are

$$P_{av} = \frac{2}{\pi} (P_p) \frac{d}{T}$$

$$= \frac{2}{\pi} (5300) \frac{0.5}{2.777} \approx 607.5 \text{ watts}$$

The rms losses are

$$P_{rms} = P_p \frac{d}{2T} = 477 \text{ watts}$$

These rms losses generate heat in the core. The heat is dissipated partly by convection and radiation to the ambient air, but the greatest part of it is dissipated by heat transfer to the cooling water flowing through the rectangular channels welded to the outer surfaces of the

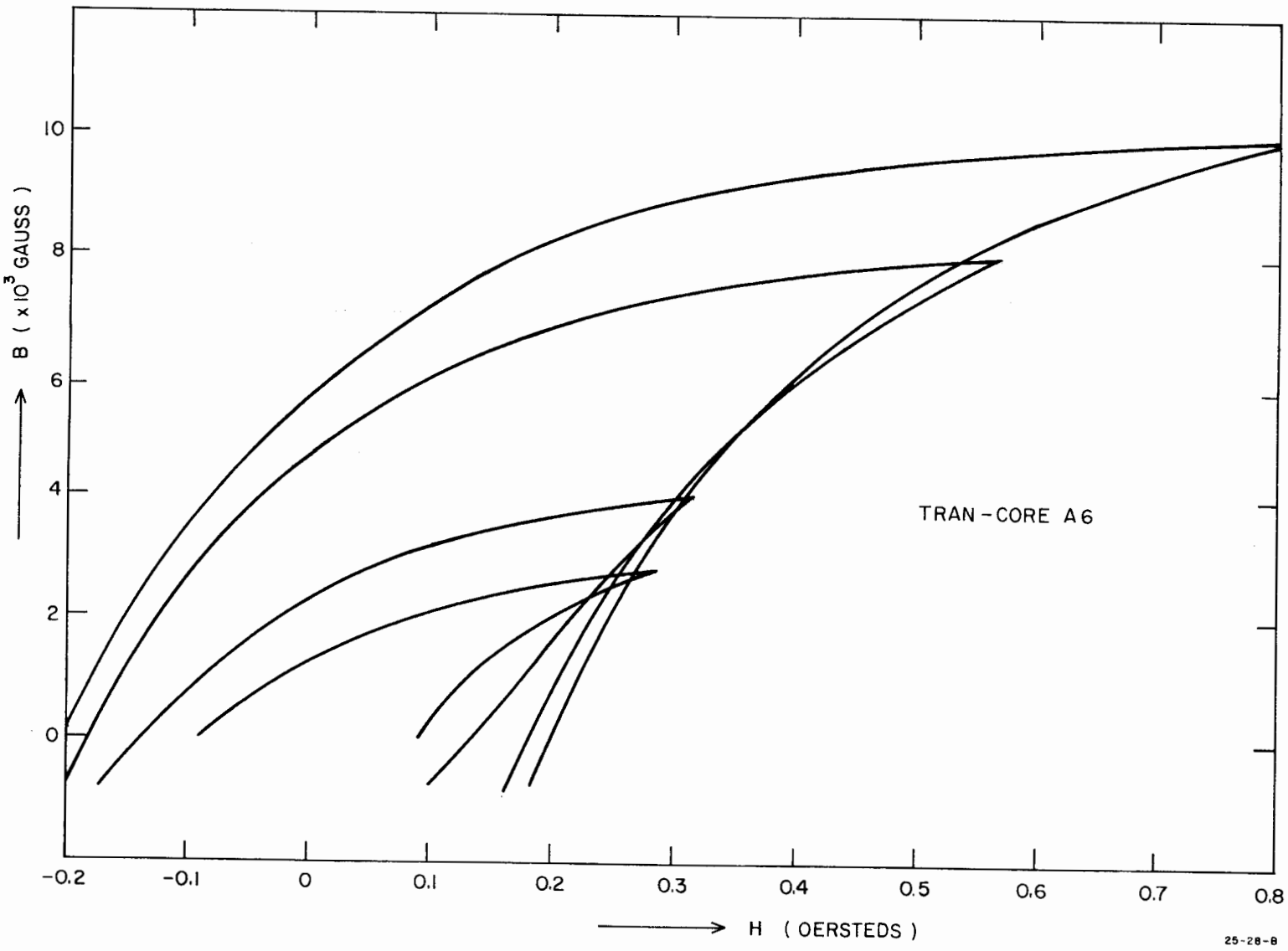

12b--Hysteresis loops of the core material chosen.

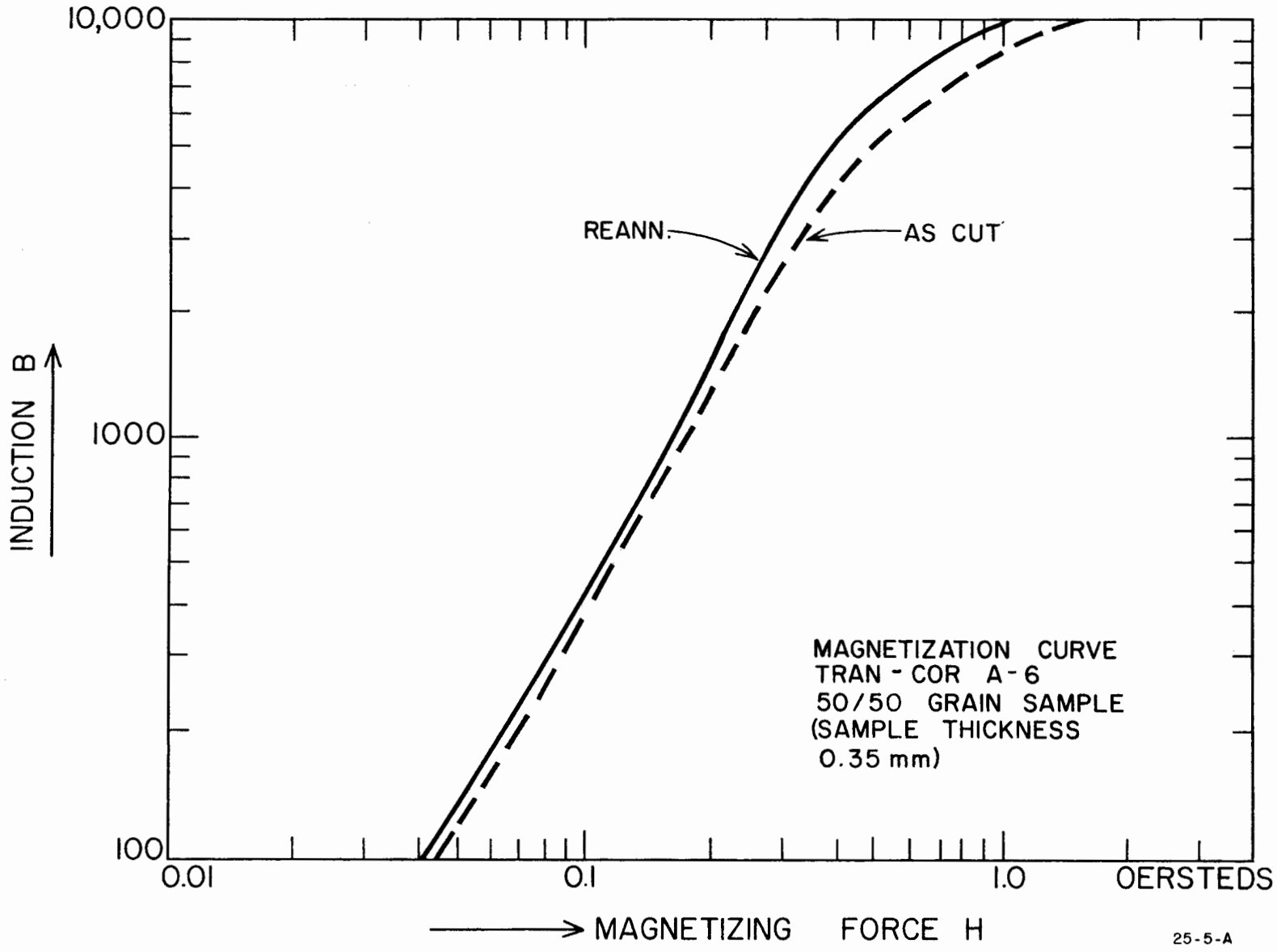

12c--Magnetization curve of the sheet material to be used in the core.

horizontal yokes. To calculate the temperature hot-spot in the core, the loss density is assumed to be uniform over the core. The temperature distribution in the core may be now calculated from the Poisson differential equation[7] for three-dimensional problems, assuming symmetric boundary conditions.

If x, y, z denote the coordinates along and perpendicular to the lamination, and w_v is the core loss density, one may write (see Fig. 13)

$$k_x \frac{\partial^2\theta}{\partial x^2} + k_y \cdot \frac{\partial^2\theta}{\partial y^2} + k_z \cdot \frac{\partial^2\theta}{\partial z^2} + w_v = 0 \qquad \text{(IV.B.2)}$$

Assuming no temperature gradient in the z-direction, the temperature distribution yields the expression

$$k_x \frac{\partial^2\theta}{\partial x^2} + k_y \frac{\partial^2\theta}{\partial y^2} + w_v = 0 \qquad \text{(IV.B.3)}$$

The solution of Eq. (IV.B.3) gives the temperature drop along the lamination inside the core $\Delta\theta_i$ and the temperature drop from the yoke surface to the bulk of the flowing water $\Delta\theta_o$:[8]

$$\Delta\theta_i = \frac{w_v}{2k_x}\left(\frac{a}{2}\right)^2 \left\{1 - 4\sum_{n=1}^{\infty}\frac{P_n}{Q_n}\left[1 - \left(n\,\frac{a}{2}\right)\right]\right\} \qquad \text{(IV.B.4)}$$

$$\Delta\theta_o = \frac{w_v}{2h_1}\,a\left[1 - \frac{2h_1}{k_x}\cdot\frac{a}{2}\sum\frac{P_n}{Q_n}\cos\left(n\,\frac{a}{2}\right)\right] \qquad \text{(IV.B.5)}$$

where h_1 denotes the surface coefficient of heat transfer from core to the cooling water, k_x and k_y are the conductivity of the sheet structure parallel and perpendicular to lamination, and a is the distance from the hot-spot temperature to the outer surface of the lamination. The term n is a Fourier coefficient expressed as

$$n\,\frac{a}{2} = \frac{h_1}{2k_x}\,a\,\cot\left(n\,\frac{a}{2}\right) \qquad \text{(IV.B.6)}$$

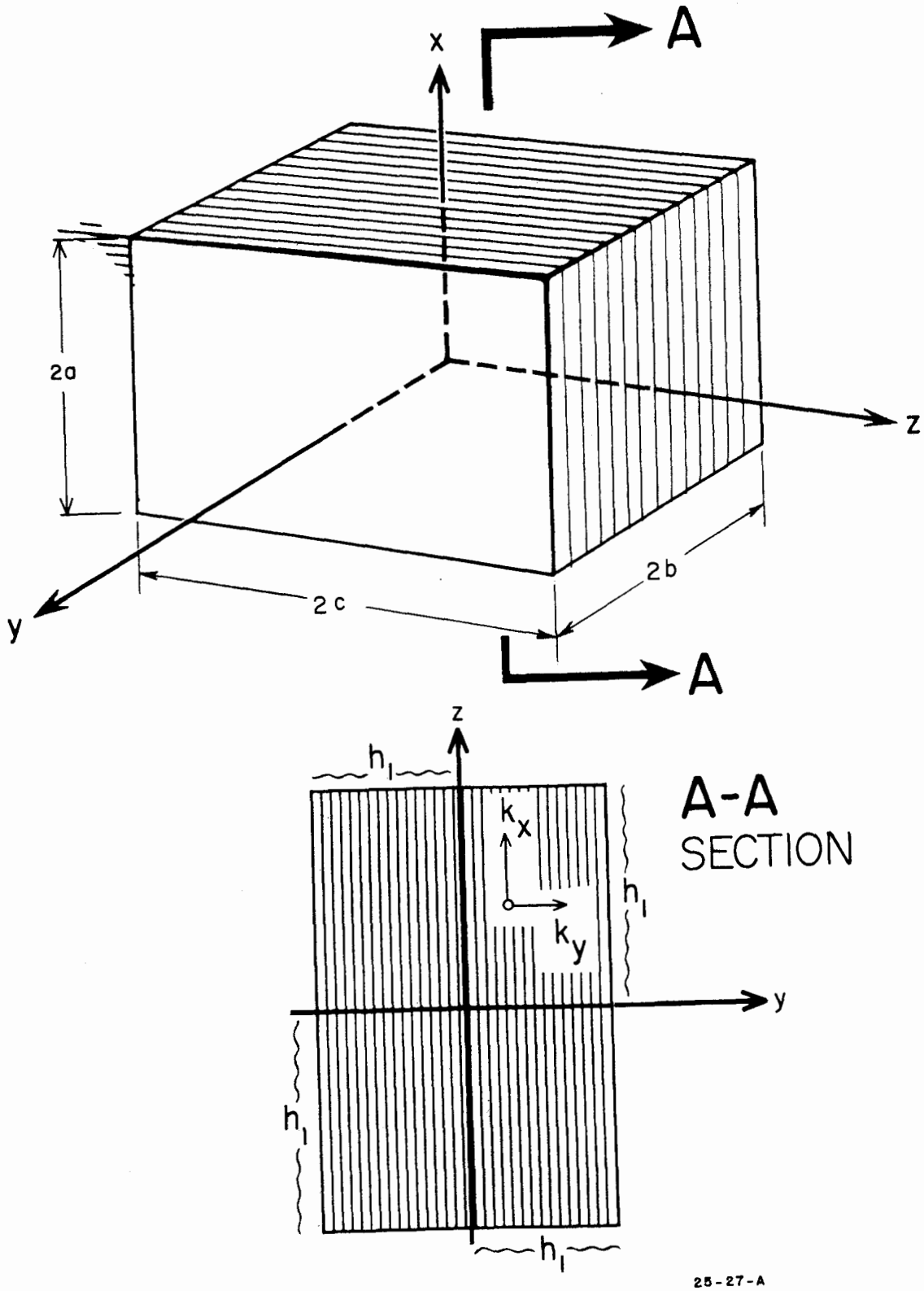

FIG. 13--Core configuration for temperature calculation.

The series P_n and Q_n are expressed as

$$P_n = \frac{\sin\left(n\,\frac{a}{2}\right)}{\left(n\,\frac{a}{2}\right)^3} \quad \frac{1}{1 + \frac{\sin(na)}{na}} \qquad \text{(IV.B.7)}$$

and

$$Q_n = \left\{1 + \frac{(k_x k_y)^{\frac{1}{2}}}{h_1} \tanh\left[\left(\frac{k_x}{k_y}\right)^{\frac{1}{2}} \left(n\,\frac{b}{2}\right)\right]\right\} \cosh\left[\left(\frac{k_x}{k_y}\right)^{\frac{1}{2}} n\,\frac{b}{2}\right] \qquad \text{(IV.B.8)}$$

The core width perpendicular to the lamination is denoted as $2b$.

The heat transfer coefficient h_1 for water over the temperature range of 5° to 100°C flowing through smooth walled tubes may be expressed, simplified, as[9]

$$h_1 = 6.76 \times 10^{-3} (1 + 0.015\,\theta_m) v_h^{0.87}\, d_n^{-0.13} \ (\text{watts/cm}^2\text{-}^\circ\text{C}) \qquad \text{(IV.B.9)}$$

The mean velocity of water is v_h, the hydraulic diameter of the cooling tube is d_h, and

$$\theta_m = 0.9\,\theta_b + 0.1\,\theta_w$$

The term v_h is expressed in cm/sec, and d_h is in cm.

The core loss density w_v calculated for our case is:

$$w_v = \left(\frac{477}{1500 \times 10^3}\right)\frac{7.65}{0.9} = 2.70 \times 10^{-3} \text{ watts/cm}^3$$

The heat conductivity perpendicular to the sheets, subjected to a pressure of 3 kg/cm^2, is

$$k_y = 0.6 \text{ Ws/meter-}^\circ\text{C}$$

and in the direction of lamination,

$$k_x = 20 \text{ weber/meter-}^{\circ}\text{C}$$

To calculate the coefficient of heat transfer, refer to Section IV.A, where a temperature rise of 10°C was estimated for the cooling water flowing through the coils. The amount of cooling water is therefore

$$Q_h = \frac{P_{\sim}}{4.186\ \Delta\theta} \text{ (cm}^3\text{/sec)} \qquad \text{(IV.B.10)}$$

With $P = 150$ watts as the rms coil losses, then

$$Q_h = 3.6 \text{ cm}^3\text{/sec}$$

Taking into account the length of the cooling tube, including the rectangular tube cooling the core, and expressing all bends in the tube, expansion and contraction losses in terms of hydraulic length, the length of the cooling path may be expressed as

$$\ell_h = 110 \text{ meters}$$

The hydraulic diameter of the cooling tube inside the cable was 3.94×10^{-3} meters. The average hydraulic diameter for the total cooling path is 4×10^{-3} meters. The velocity of water is therefore

$$v_h = 0.34 \text{ meters/sec}$$

The pressure drop of water inside smooth tubes may be expressed as

$$\Delta p = 5 \times 10^{-5} \ell_h \left(\frac{v_h^{1.75}}{d_h^{1.25}} \right) \text{(kg/cm}^2\text{)} \qquad \text{(IV.B.11)}$$

The d_h and ℓ_h are expressed in meters, and v_h in meters/sec. Thus, the pressure drop, with the above calculated values of ℓ_h and v, is

$$\Delta p \approx 0.75 \text{ kg/cm}^2$$

The bulk water temperature rise cooling the core would be, with the above value of $Q = 3.6$ cm^3/sec, about 25°C. By using the available pressure drop of $\Delta p = 5$ kg/cm^2, one obtains

$$v_h \approx 1 \text{ meter/sec}$$

and

$$Q = 12.6 \text{ cm}^3/\text{sec}$$

$$\Delta\theta_{coil} = 3.4^\circ\text{C}$$

The cooling water cools first the lower part of the core, then passes through the coil; after cooling the upper part, it flows back to the heat exchanger.

The temperature rise of water after cooling the lower part of the core is

$$\Delta\theta_1 = 4.6^\circ\text{C}$$

The total water temperature rise is

$$\Delta\theta_h = 4.6 + 3.4 + 4.6 = 12.6^\circ\text{C}$$

The water inlet temperature is about 40°C. The coefficient of heat transfer for the lower part of the core may be estimated as

$$\theta_b = 43^\circ$$

$$\theta_w = 45^\circ\text{C}$$

$$h_1 = 1.3 \text{ watt/cm}^2\text{-}^\circ\text{C}$$

and for the upper part of the core,

$$\theta_b = 46.5^\circ C$$

$$\theta_w = 50^\circ C$$

$$h = 1.5 \text{ watt/cm}^2\text{-}^\circ C$$

From Fig. 2 the length of $a = 0.27$ meter was estimated, which means that the core hot-spot is near the pole tip. Now, from Eqs. (IV.B.4) and (IV.B.5) it may be seen that

$$\Delta\theta_i = 2.5^\circ C$$

$$\Delta\theta_{o,\ell} = 0.1^\circ C$$

$$\Delta\theta_{o,u} = 0.1^\circ C$$

Due to small slipping of sheets with respect to each other, during stacking a gap between the wall of the rectangular cooling tube and the core surface may occur. This gap leads to a higher temperature gradient over the tube surface. The gap between cooling tube and core surface will be filled with epoxy in order to increase the heat conductivity in this gap. A maximum gap of 5×10^{-2} cm (0.020 inches) is estimated, and with a thermal conductivity of $k = 0.015$ watt/cm-$^\circ$C, $\Delta\theta_g = 20^\circ C$.

The total temperature rise over the magnet is, according to the above calculation,

$$\Delta\theta_{max} = 4.6 + 3.4 + 4.6 + 2 \times 2.5 + 2 \times 0.1 + 20 = 37.8^\circ C$$

The hot-spot temperature with a water inlet temperature of $40^\circ C$ would then be

$$\theta_{hs} = 77.8^\circ C$$

In the above calculation the effect of heat radiation has been neglected.

V. PULSER INDUCTANCE

A. Basic Parameters

The inductance to be used in the pulser circuit was mentioned in Section I. The current of opposite polarity to the current flowing through the magnet passes through the inductance, and therefore the inductance must have nearly the same impedance as the magnet. The design parameters of the inductance must therefore be

$$U_p = 4200 \text{ volts}$$

$$L \approx 2 \times 10^{-3} \text{ henry}$$

$$E = 106 \text{ joules}$$

The peak current flowing through the inductance would be 316 amps.

B. Type of Inductance

Besides matching the required data, the inductance had to have the highest Q-value possible. From different design possibilities, the iron-bound solution shown in Fig. 14 was chosen. The laminated core is built from cold rolled grain-oriented sheets in lap-joint construction. The coil is placed inside the window and has an air gap. The field pattern, the distribution of the flux lines, and the distribution of the ampere turns over the coil are shown schematically in Fig. 15. The inductance may be calculated for this configuration from the magnetic energy,

$$E_m = \frac{1}{2} \mu_o \int H^2 \, dV \qquad \text{(V.B.1)}$$

With the assumption of uniform current distribution inside the window, the relation

$$\frac{H}{i} = \frac{N}{h} \qquad \text{(V.B.2)}$$

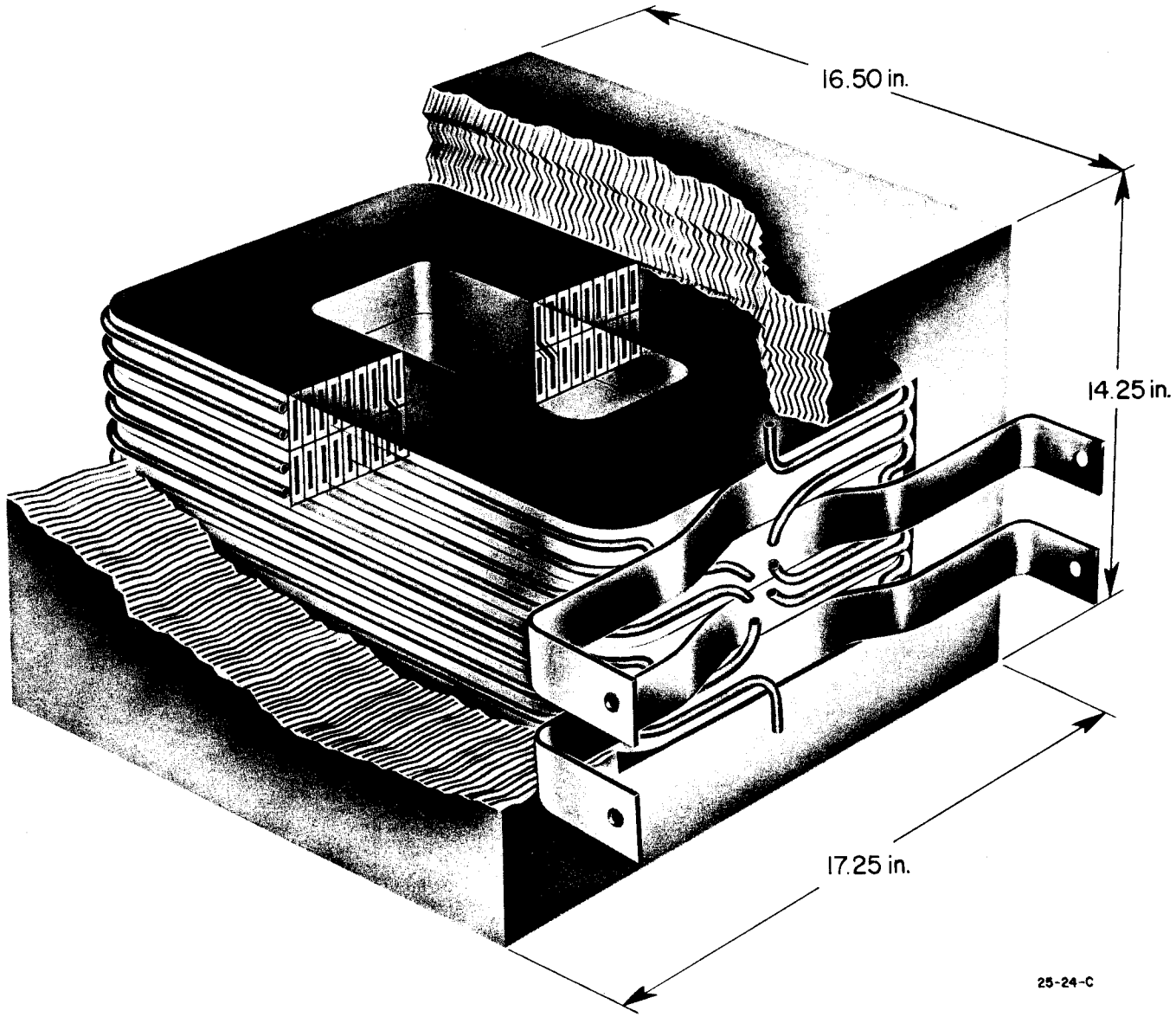

FIG. 14--Pulser inductance.

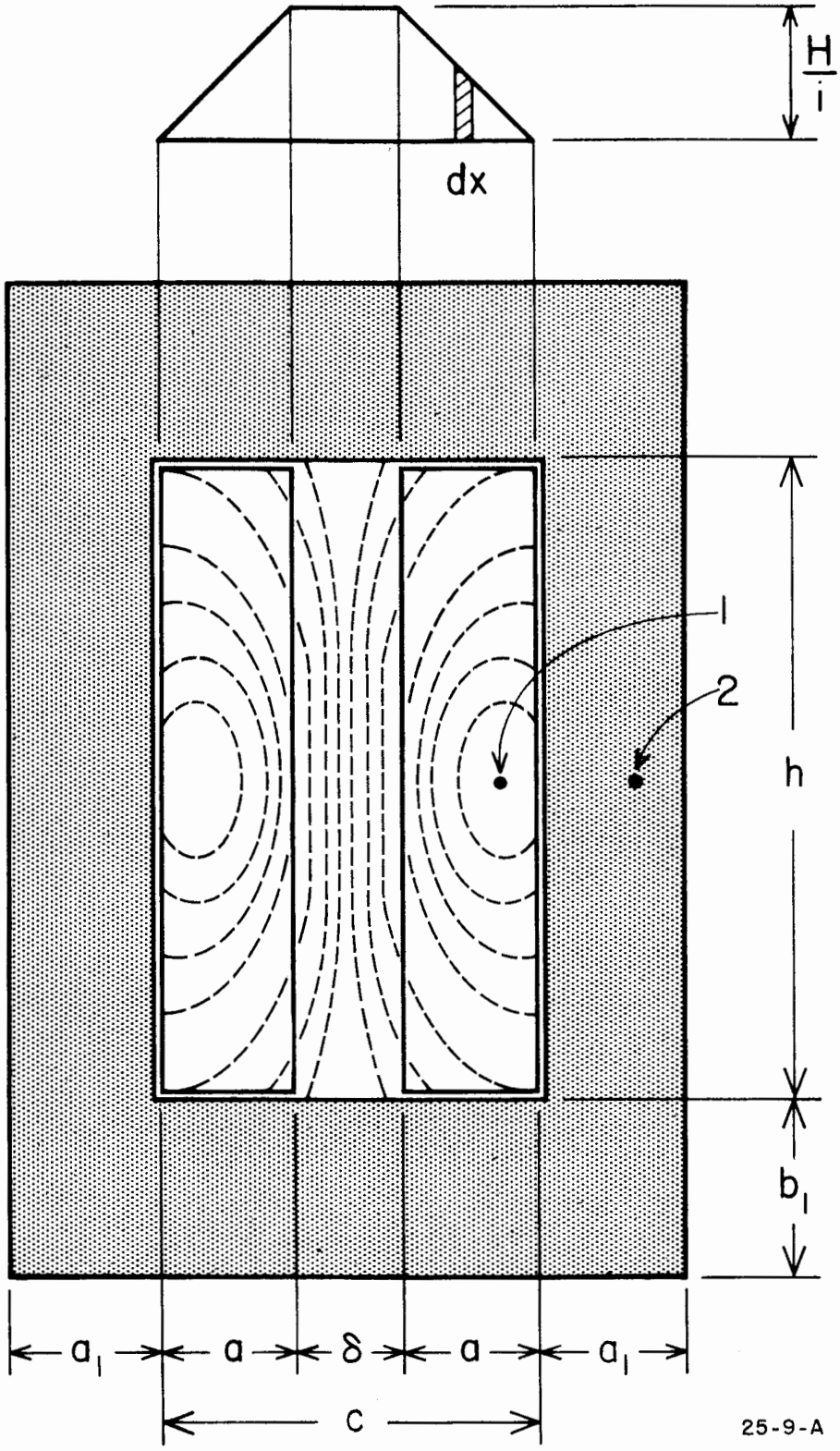

FIG. 15--Schematic field and amp-turn-pattern of the inductance.

is valid. Introducing the ideal magnetic reluctance, Λ, results in

$$\Lambda = \frac{1}{N^2 i^2} \mu_o \int H^2 \, dV \qquad \text{(V.B.3)}$$

and

$$L_1 = N^2 \Lambda \qquad \text{(V.B.4)}$$

The relations (V.B.1) through (V.B.4) are true only if the magnetic energy in the core is neglected. The integration of Eq. (V.B.4) gives the inductance as

$$L = \mu_o \left(\frac{\ell_m N^2}{h}\right) \left(\delta + \frac{2}{3} a\right) \qquad \text{(V.B.5)}$$

If the coil does not completely fill the window, a correction factor k (known as the Rogowsi factor) has to be introduced in Eq. (V.B.5):

$$L = \mu_o \ell_m \frac{N^2}{h} k \left(\delta + \frac{2}{3}\right) \qquad \text{(V.B.6)}$$

The relation between k and the number κ is illustrated in Fig. 16, where

$$\kappa = \frac{h}{2} (\delta + 2a) \qquad \text{(V.B.7)}$$

In order to be able to have a pulser inductance with the possibility of choosing different L values, the coil was split into four sections. Each section is built as a pancake and two pancakes are internally connected in series to form a double pancake. Each inductance consists of two double pancakes placed on top of each other and may be connected in series or parallel according to the requirements. Each pancake consists of flat copper strips with a thin (0.007 inch) insulation strip between adjacent turns. Two conductors are connected in parallel and the transition from the upper to the lower

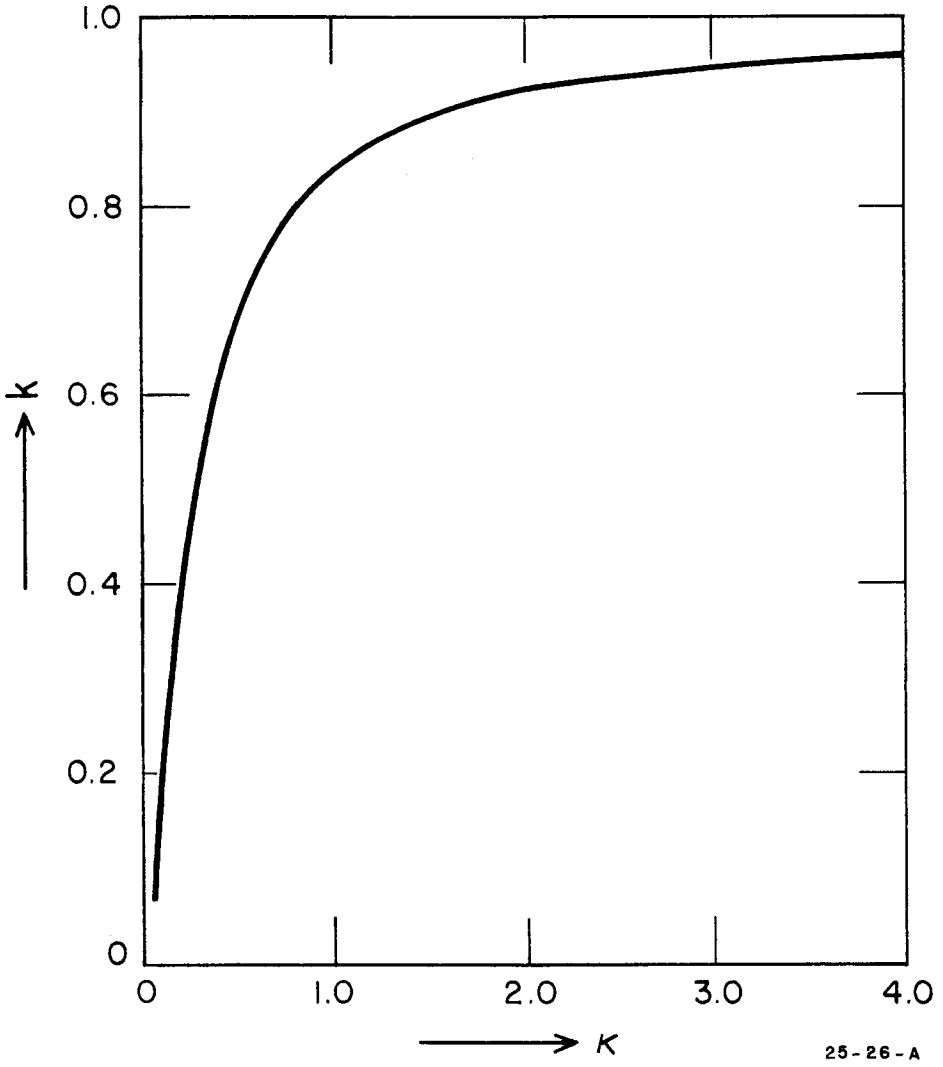

FIG. 16--Correction factor k as a function of κ.

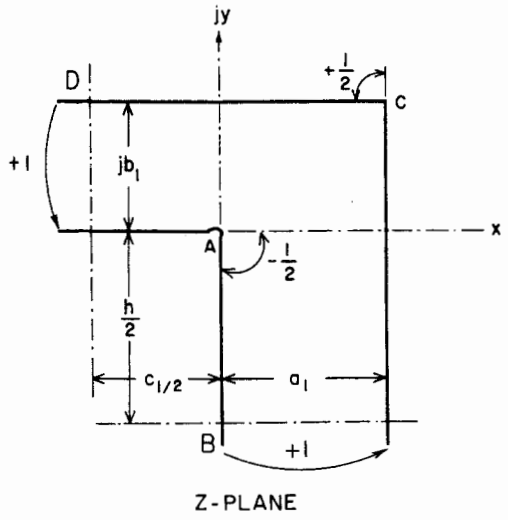

Z-PLANE

(a)

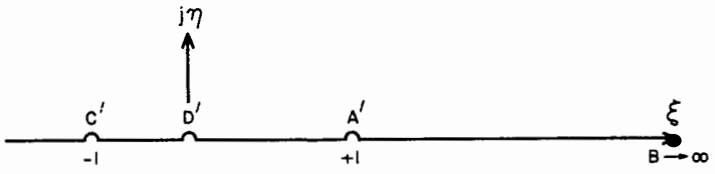

t-PLANE

(b)

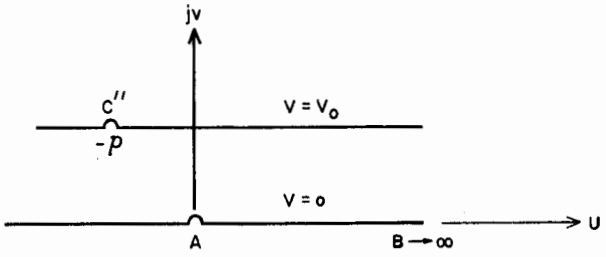

W-PLANE 25-25-A

(c)

Flux density:

$$B_x - jB_y = jB_o \left[\frac{t + \left(\frac{a_1}{b_1}\right)^2}{t - 1} \right]^{\frac{1}{2\theta}}$$

Iron length:

$$\ell_{F_e} = 2 \left[h + c_1 \left[\left(\frac{b_1}{a_1}\right)^{1-\theta} - \left(\frac{2b_1}{\delta}\right)^{1-\theta} \right] + \left(0.92 + 0.16 \frac{b_1}{a_1}\right) a_1 + \left(0.92 + 0.32 \frac{b_1}{\delta}\right) \delta \right]$$

Core losses:

$$P_{F_e} = p_{F_e} \cdot \gamma \cdot A \cdot \ell_{F_e}$$

FIG. 17--Schematic core configuration.

P_{F_e}, the mean flux density in the core must first be known. From

$$\Phi = \frac{LI}{N} = \frac{2.4 \times 10^{-3} \times 340}{102} = 8.10^{-3} \text{ (weber)}$$

$$B_o = \frac{\Phi}{2A} = 0.175 \text{ wb/meter}^2$$

with $f = 10^3 \text{ sec}^{-1}$ and $B = 0.175 \text{ wb/meter}^2$, the loss density p_{F_e} in the direction of grain orientation may be calculated for the sheet materials below:

ARMCO M6 (0.35-mm): $p_{F_e} = 2.30$ watts/kg

and

Allegheny Ludlum AL 4750 (0.35-mm): $p_{F_e} = 1.35$ watts/kg

It may be noted that Eq. (V.C.1) is exact for hot rolled sheets without grain orientation. The specific losses parallel and perpendicular to the rolling direction differ only about 10% maximum for sheets with the lowest loss factors, but are considerably different for grain-oriented sheets. In those sections where core and yoke sheets are overlapped, the flux direction has to deviate from the rolling direction. The divergence between flux and rolling direction causes additional core losses. Figure 18 shows the variation of specific core losses for a flux density of $\approx 0.2 \text{ wb/meter}^2$ in grain-oriented sheets and the magnetization force as a function of the divergence angle between flux and rolling direction.

A further increase in the loss factor comes from cutting the sheets and stacking and pressing the core. A nonuniform compression may increase the losses for this low flux density up to 6%.

Combining the above factors, one may write Eq. (V.C.1) in the form

$$P_{F_e} = 2\left(p^{*}_{F_e}\right) \gamma \left[h + c \left[\left(\frac{b_1}{a_1} \right)^{1-\theta} - \left(\frac{2b_1}{\delta} \right)^{1-\theta} \right] + \left(0.92 + 0.16 \frac{b_1}{a_1} \right) a_1 + \left(0.92 + 0.32 \frac{b_1}{\delta} \right) \delta \right] \qquad \text{(V.C.2)}$$

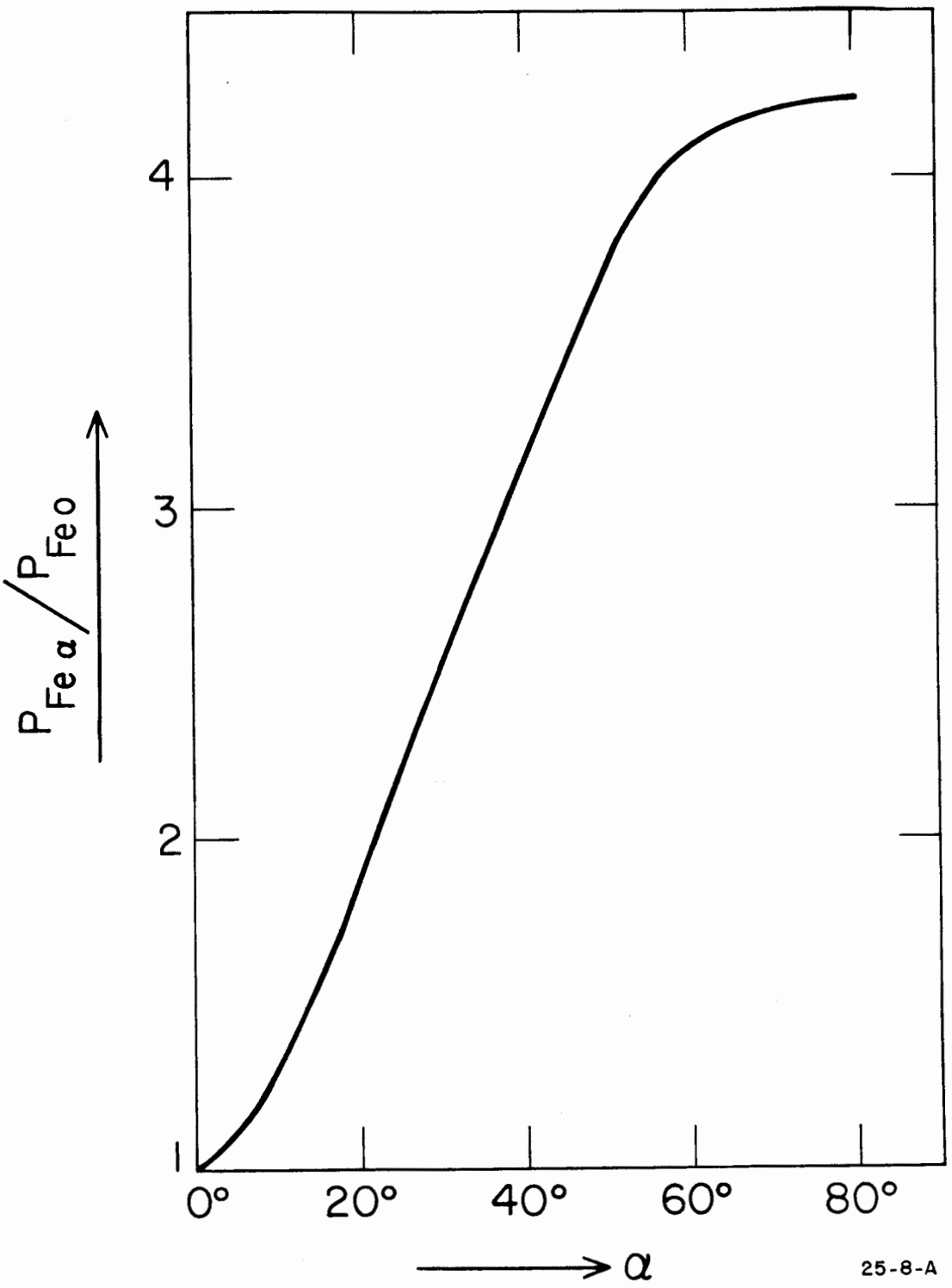

FIG. 18--Variation of loss factors as a function of the angle between flux direction and rolling direction.

For our particular core, the specific losses are

$$p'_{F_e} = 2.5 \text{ watts/kg} \quad \text{(Armco M6)}$$

and

$$p'_{F_e} = 1.53 \text{ watts/kg} \quad \text{(A.L. 4750)}$$

The core losses are therefore calculated as

$$P_{F_e} \approx 2000 \text{ watts} \quad \text{(Armco M6)}$$

$$P_{F_e} \approx 1230 \text{ watts} \quad \text{(A.L. 4750)}$$

The average losses (see Section III) are

$$P_{F_e} \text{ rms} = 2 \times 10^3 \times \frac{0.5}{2 \times 2.778} = 180 \text{ watts} \quad \text{(Armco M6)}$$

$$P_{F_e} \text{ rms} = 111 \text{ watts} \quad \text{(A.L. 4750)}$$

The temperature calculation according to Eqs. (IV.B.4) and (IV.B.5) showed that it is not necessary to use water cooling for the core. The core is cooled by natural convection.

D. The Coil

The coil inside the iron frame is subjected to the pulsed field. The most important part of the losses in the coils are those influenced by skin and proximity effects. Several investigators have attacked this problem[11] and the conclusions of their work will be used in this paper.

It can be shown that Eq. (IV.A.3) is also useful for this particular case, but it must be slightly adjusted to our application.

The coil is wound with two copper strips parallel. The strips are interleaved in the transition part from the upper to the lower pancake (see detail Fig. 15). It was found that hollow water-cooled conductors could not be used due to the high eddy current losses. The conductor consists of two high conductivity OFHC copper strips with dimensions of 0.054×3.04 cm^2 each. The number of layers in a pancake across the field direction is $m = 51$. The mean conductor length is 0.73 meter.

The dc resistance of the coil is (with two double pancakes connected in parallel)

$$R = 2.10^{-6} \frac{102 \times 73}{2 \times 2 \times 5.04 \times 10^{-2} \times 3.04}$$

$$= 1.97 \times 10^{-2} \text{ ohm}$$

The coil resistance in the ac magnetic field, decreasing from maximum value to zero, may be calculated in the following way.

The function x from Eq. (IV.A.4) can be modified here in a more suitable form,

$$x = 2\pi \Delta \left(\frac{na}{c}\right) f \kappa \times 10^{-9} \qquad \text{(V.D.1)}$$

The resistance ratio from Eq. (IV.A.3) can be written in the simple form,

$$\frac{R_\sim}{R_=} = 1 + \frac{m^2}{36} x^4 \qquad \text{(V.D.2)}$$

where:

Δ = conductor thickness across the field
n = number of axial turns
c = axial height of the coil
m = number of turns across the field

In our case, $\Delta = 0.054$ cm and $m = 102$ (2 copper strips parallel), so

$$x = 2\pi \times 5.04 \times 10^{-2} \left[\frac{(4)(3.04)(10^{3})(10^{-9})}{(17.3)(2)(10^{-6})} \right]$$

$$= 2.05 \times 10^{-1}$$

and the resistance ratio is

$$\frac{R_{\sim}}{R_{=}} = 1 + \frac{1.04 \times 10^{4}}{36} \quad (18.4)(10^{-4}) = 1.51$$

The total coil resistance is:

$$R_{\sim} = 2.975 \times 10^{-2} \text{ ohms}$$

The rms copper losses are therefore

$$P_{F_e} \text{ rms} = I_p^2 R_{\sim} \left(\frac{d}{2T} \right)^{\frac{1}{2}} = 267 \text{ watts at } 60^{\circ}\text{C}$$

Each double pancake is impregnated under vacuum with a low viscosity epoxy of temperature class F. The glass fiber insulation between adjacent copper sheets is extended axially on both sides between pancakes and adjacent turns. Around the coil enough insulation to ground is foreseen to prevent flashover to the grounded core.

If perfect impregnation of each coil is assumed and the heat conductivity parallel to the coil axis is neglected, forcing the heat to flow perpendicular to the lamination, the maximum temperature rise from the cooling water to the hot-spot can be calculated from Eqs. (IV.B.4) and (IV.B.5).

The thermal conductivity of epoxy-impregnated glass fiber is $k_x = 0.62$ watt/meter$^{\circ}$C, and the thermal conductivity of a copper and

insulation structure is

$$k_{res} = \frac{\sum_{i} d_i \left(\pi_{k_i} \right)_i}{\sum_{\substack{i,k \\ i \neq k}} \left[d_i \left(\pi_{k_k} \right)_k \right]} \qquad \text{(V.D.3)}$$

$$i = 1 \ldots n$$

$$k = 1 \ldots n$$

which gives in our case,

$$k_{res} = \frac{(d_{ins} + d_{cu})\, k_{ins}\, k_{cu}}{d_{in}\, (k_{cu} + d_{cu})\, k_{ins}} = 2.38 \text{ watt/meter}^{\circ}\text{C}$$

The coil power density is

$$w_v = \frac{267}{4900} = 0.054 \text{ watt/cm}^3$$

which gives

$$\Delta\theta_i \approx \frac{w_v}{2k_{res}} \left(\frac{a}{2}\right)^2 = \frac{0.054}{(2)(2.38)(10^{-2})} \left(\frac{8}{2}\right)^2 = 18.2^{\circ}\text{C}$$

The cooling tubes brazed on the coil surface have a hydraulic diameter of 0.45 cm and a length of 62.5 cm. The plastic tubes connecting the cooling tubes of each pancake to the other have a length of 20 cm. Calculating now the entry and exit losses of water and the pressure losses due to the bends, expressing them in terms of tubing length, we get for the length of the cooling tube

$$\ell_h = 8 \text{ meters}$$

The amount of water required for a temperature rise of $5^{\circ}C$ of the bulk water cooling the coils is

$$Q_h = 1.275 \times 10^{-2} \text{ liters/sec}$$

and the pressure drop over the dummy load is

$$\Delta p \approx 1.0 \text{ kg/cm}^2$$

The heat transfer coefficient is calculated from Eq. (IV.B.9):

$$h_1 = 0.55 \text{ watts/cm}^2 \, ^{\circ}C$$

The temperature drop from the coil surface to the water bulk temperature is therefore

$$\Delta\theta_o = \frac{w_v a}{2h} = \frac{(0.054)(8)}{1.1} \approx 0.5^{\circ}C$$

If, due to coil manufacturing difficulties, a gap of 0.1 – 0.2 cm is assumed between the last conductor layer that is soldered to the cooling tubes and the rest of the coil, another temperature drop of

$$\Delta\theta_{ins} = \frac{w_s \, d_{is}}{k} \qquad \text{(V.D.4)}$$

$$w_s = \frac{267}{(3)(75)(4)} = 0.3 \text{ watt/cm}^2$$

$$\Delta\theta_{ins} = \frac{(0.3)(0.2)}{0.6 \times 10^{-2}} = 10^{\circ}C$$

is obtained.

The water temperature at the entrance of the pulser inductance is assumed

to be 40°C. The hot-spot temperature is therefore

$$\theta_{hs} = 40 + 18.2 + 0.5 + 10 = 68.7^{\circ}C$$

In this calculation the heat conductivity along the conductors and the heat radiation are neglected.

TABLE III

Dummy Load

(Calculated Values)

Inductance	2.0×10^{-3} henry
Energy	106 joules
Peak voltage	316 amps
Coil ac resistance	3×10^{-2} ohms
Equivalent core resistance	$2. \times 10^{-2}$ ohms
Total ohmic losses (rms)	447 watts
Temperature rise in water	5°C
Amount of water	0.8 liters/minute
Pressure drop over the dummy load	1.0 kg/cm^2
Coil hot-spot	68.7°C
Number of series turns per pancake	51
Number of pancakes	4
Parallel conductors per turn	2
Conductor dimensions	0.054×3.04 cm^2
Mean turn length	0.73 meter
Weight of copper	44 kg
Weight of iron	210 kg
Total weight	275 kg

VI. APPENDICES

APPENDIX A

The Noise Calculation of the Core

The magnet core may be considered as the main noise source. It is known that the noise level changes with the flux density in the core. However, the exact cause for the generation of noises in the core is not known; it is generally agreed that this may be due to magnetostrictive effects on individual sheets. The vibration caused by expansion and contraction of sheets generates noise. From tests it is known that the noise level in a core with butt joints is generally higher than in those with lap joints. In the present magnet it was not possible to use lap-joint design. The relative change in the sheet length in the field direction $\frac{\Delta \ell}{\ell}$ is a function of the core flux density.[12] The flux density in the core is not constant, but varies due to the fringing field effect from the pole tip toward the horizontal yokes. The flux density in the yokes is different also from the average value in the yoke corners. However, to simplify the calculation, only the maximum flux density in the core is used. For an infinitely extended sheet, oscillating with an amplitude under the influence of the magnetostriction, the power per unit area may be expressed as[13]

$$P_1 = 83\ \pi^2\ f^2\ X^2\ (10^{-7})\ \text{watts/cm}^2 \qquad \text{(VI.A.1)}$$

The noise level is defined generally in terms of two powers:

$$L = 10 \left(\log_{10} \frac{P_1}{P_2} \right) \text{dB} \qquad \text{(VI.A.2)}$$

The power equivalent at 1000 cps is correlated to a threshold value of

$$P_2 = 10^{-16}\ \text{watts/cm}^2$$

Combining now the above equations yields

$$L = 10 \log_{10} (820\ f^2\ X^2 \times 10^9)\ \text{dB} \qquad \text{(VI.A.3)}$$

Neglecting the higher harmonics, the maximum deflection may be expressed as

$$X = \frac{\Delta l}{2}$$

and therefore the corresponding frequency is two times the pulse repetition rate. The relation between the relative change of the sheet length and the flux density is shown in Fig. 19.

For a yoke length of $l = 100$ cm and a maximum induction of $B = 3000$ gauss, one obtains

$$\frac{\Delta l}{l} = 0.12 \times 10^{-6}\ ; \qquad \Delta l = 1.2 \times 10^{-5}\ \text{cm}$$

Therefore:

$$X = 6.0 \times 10^{-6}\ \text{cm}$$

For:

$$f = 720\ \text{sec}^{-1}$$

The noise level is

$$L = 10 \cdot \log_{10} (820 \times 5.18 \times 10^4 \times 36 \times 10^{-12} \times 10^9)$$

$$= 11\ \text{dB}$$

This level is quite low. However, for higher saturated cores, it is important to reduce the flux density in the butt joint. Possible and simple solutions are given in Fig. 20.

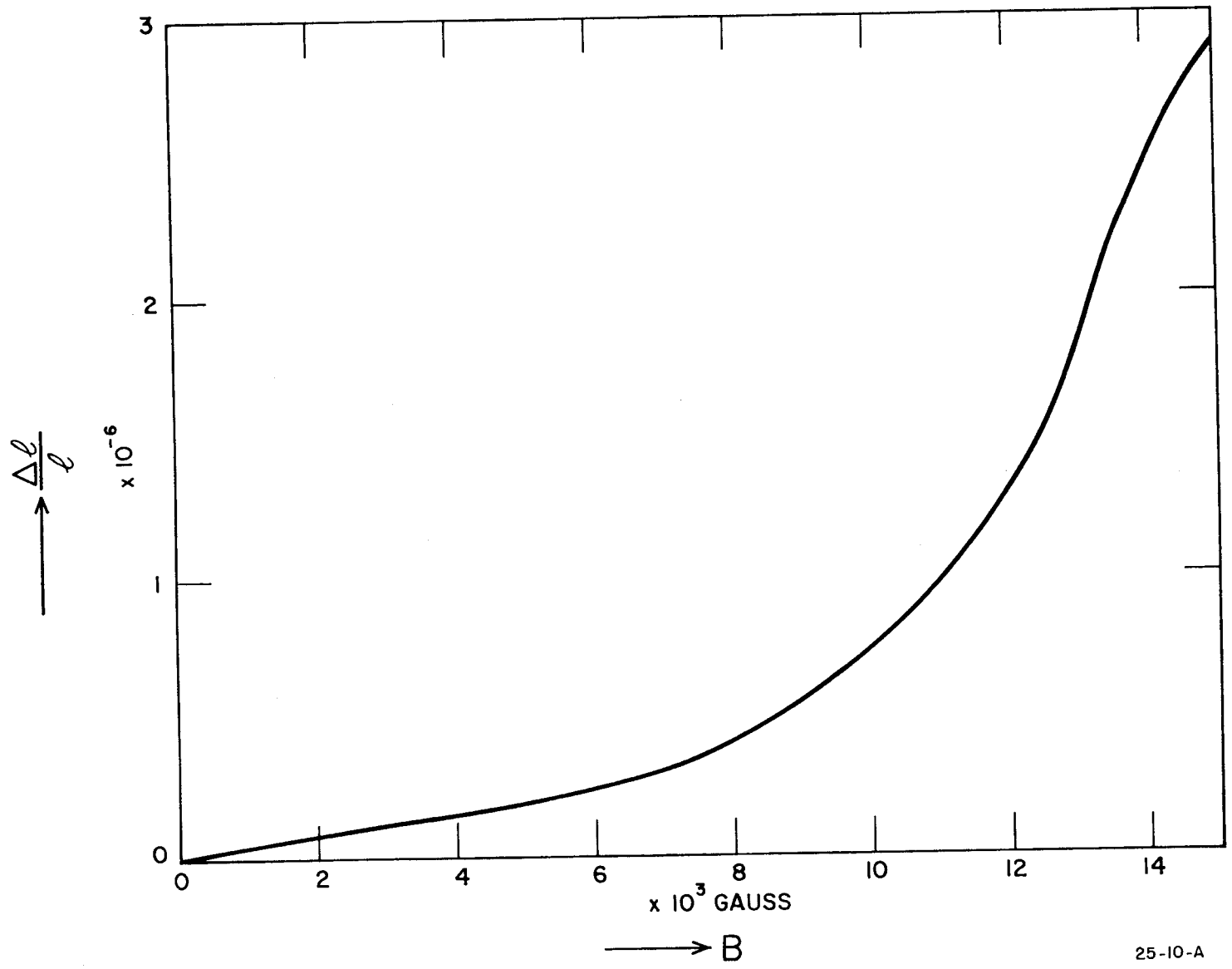

FIG. 19--Relative change in sheet length as a function flux density in the core.

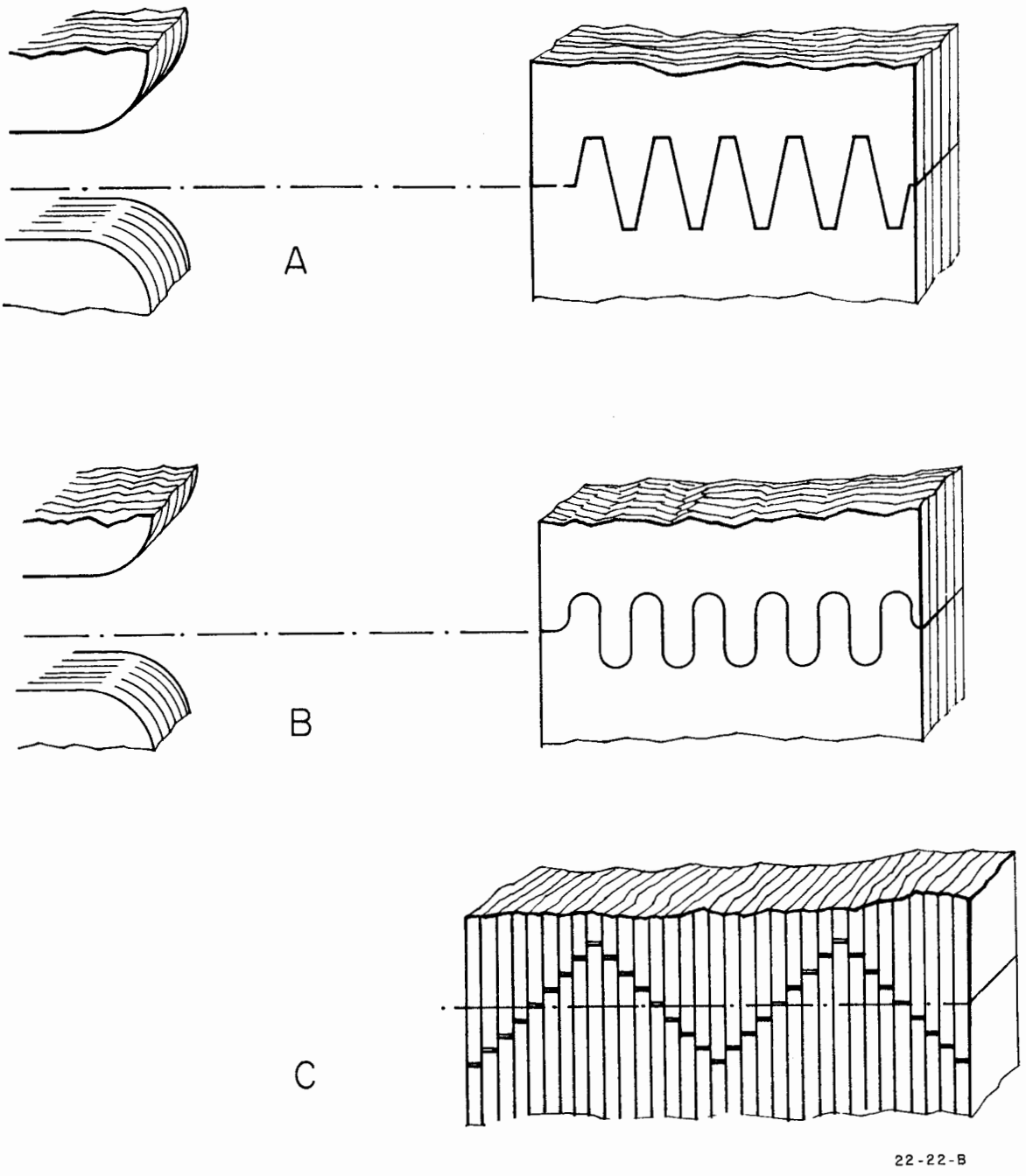

FIG. 20--Butt joint configuration in core.

APPENDIX B

The Quality Factor of the Circuit

Because of the resistance of the different pulser components, the circuit has losses. The quality factor Q may be calculated for sine wave pulses from the relation

$$Q = \frac{4\pi \cdot f \cdot E_{rms}}{P_{rms}} \qquad \text{(VI.B.1)}$$

which leads to

$$Q = \frac{\omega \sum_i L_i}{\sum_i R_i} \qquad \text{(VI.B.2)}$$

$$i = 1 \ . \ . \ . \ n$$

The internal resistance of the capacitors as well as the voltage drop along the connections in the pulser are neglected. The losses in the magnet, the inductance, the cable from the capacitor bank to the magnet, and the voltage drop across the firing gates (ignitrons) are considered. The magnet resistance was calculated in Section III to be

$$R_m = 6.96 \times 10^{-2} \text{ ohms}$$

The equivalent resistance of the inductance L was calculated in Section V as

$$R_L = 5 \times 10^{-2} \text{ ohms}$$

The cable from the pulser to the pulsed magnet has a length of 122 meters. The leads consist of two parallel shielded coaxial multistranded cables of type 250 Mem. The cable has an inductance of 8.5×10^{-6} henry and a resistance of 17.9×10^{-3} ohms.

The voltage drop across each ignitron is estimated to be 18 volts, which is equivalent to a resistance of 5.7×10^{-2} ohms.

The magnet inductance was calculated to be

$$L_m = 2.1 \times 10^{-3} \text{ henry}$$

and of the inductance,

$$L_i = 2.0 \times 10^{-3} \text{ henry}$$

With Fig. 2 and Eq. (VI.B.1), the quality factor for each half of the pulser circuit is found to be

$$Q = \frac{2\pi \times 10^3 \times (2.1 \times 10^{-3} + 2.0 \times 10^{-3} + 8.5 \times 10^{-6})}{6.96 \times 10^{-2} + 5 \times 10^{-2} + 1.79 \times 10^{-2} + 2 \times 5.7 \times 10^{-2}}$$

$$Q \approx 100$$

From $E_{rms} = 70$ joules, $P_{rms} = 7.6 \times 10^3$ watts, again $Q = 100$.

APPENDIX C

Effect of Core Dimensional Changes Due to Heating on $\int Bd\ell$

As calculated in Section III, the core temperature changes due to eddy current and hysterisis losses in the iron sheets. Due to the temperature rise in the core, the vertical yokes expand, which leads to a larger gap width as well as changes in the core dimension along the beam. The change may be expressed

$$\int Bd\ell = (B_o \ell_{eff}) \rightarrow (B_o - \delta B_o)(\ell_{eff} + \delta \ell_{eff})$$

$$\approx B_o \ell_{eff} - \delta B_o \ell_{eff} + B_o \delta \ell_{eff}$$

Second-order changes have been neglected.

$$\delta \ell_{eff} = \alpha \, \Delta\theta \, \ell_{eff}$$

and

$$\delta B_o = \alpha \, \Delta\theta B_o$$

with α as the expansion coefficient of the sheets

$\int Bd\ell$ remains unchanged.

APPENDIX D

The Temperature Rise in the Cable

The cable losses are calculated from the relation

$$P = (I_{rms})^2 \times R_{cable}$$

For pulses of full sine waves, the rms current is

$$I_{rms} = I_p \times \sqrt{\frac{6d}{2T}}$$

$$= 235 \text{ amps}$$

With the cable losses of (cable type 500 Mcm)

$$P_{cable} = 990 \text{ watts}$$

and assuming that half the cooling surface is exposed to air, the losses per unit cooling surface are seen to be

$$w_s = 4.5 \times 10^{-3} \text{ watt/cm}^2$$

The temperature rise inside the cable across the insulation is calculated from the equation

$$\Delta\theta = \frac{w_s \, d_{ins}}{k_{ins}} \qquad \text{(VI.D.1)}$$

with

$$k_{ins} = 3.34 \times 10^{-3} \text{ watt/cm-}^{\circ}\text{C} \quad \text{(polyethylene)}$$

$$d_{ins} = 0.63 \text{ cm}$$

$$\Delta\theta \approx 1^{\circ}\text{C}$$

The temperature rise from ambient air to the cable surface may be

calculated from[19]

$$\Delta\theta_{b_1} = \frac{k_{air}}{D_{cable}} h_c \qquad \text{(VI.D.2)}$$

with:

$$C_{Nu} = (C_{GR}\, C_{PR}) \qquad \text{(VI.D.3)}$$

$$C_{GR} = \frac{D_c^3\, \rho\, g\beta\Delta\theta}{\nu^2} \qquad \text{(VI.D.4)}$$

$$C_{PR} = \left(\frac{c_p \cdot \mu}{k}\right)_{air} \qquad \text{(VI.D.5)}$$

With:

$D_c = 4 \times 10^{-2}$ meter for the cable o.d.

and

$k = 0.10$ watt/meter-^oC

$c_p = 10^3$ watt/kg-^oC

$\mu = 19 \times 10^{-6}$ kg/meter-sec

$\rho = 1.22$ kg/meter^3

$\nu = 16 \times 10^{-6}$ meter^2/sec

$g = 9.81$ meter/sec^2

$\beta = 1/273$

for air one obtains

$$C_{GR} = 1.1 \times 10^5$$

$$C_{PR} = 0.19$$

and the Nusselt number,

$$C_{Nu} = 2 \times 10^4$$

The heat transfer coefficient for horizontal cylinders in air is obtained from the correlation

$$h_c = 2.237 \times 10^{-4} \left(\frac{\Delta\theta_{b_1}}{D_c} \right)^{0.25} \qquad \text{(VI.D.6)}$$

with

$$\Delta\theta_{b_1} = \frac{w_s}{h_c} \qquad \text{(VI.D.7)}$$

Combining Eqs. (VI.D.6) and (VI.D.7) yields

$$\underline{\Delta\theta_{b_1} = 8.4 \times 10^2 \, w_s^{0.8} \times D_c^{0.2}} \qquad \text{(VI.D.8)}$$

With the values of heat flux w_s and D_c given above, it can be seen that

$$\Delta\theta_{b_1} = 17.45^{\circ}C$$

or the total temperature gradient of

$$\Delta\theta_c = 18.45^{\circ}C$$

LIST OF REFERENCES

1. J. L. Cole, B. Hedin, and J. J. Muray, "Model pulsed magnet," Internal Document, Stanford Linear Accelerator Center, Stanford University, Stanford, California (January 1963).
2. B. Hedin, "A bending magnet with non-saturating shimming," SLAC Report No. 19, Stanford Linear Accelerator Center, Stanford University, Stanford, California (September 1963).
3. J. D. Cockroft, "The effect of curved boundaries on the distribution of electrical stress round conductors," Journal I.E.E. 66, 385 (1928).
4. H. Brechna, B. Hedin, and J. Cobb, "The effect of pole shimming on the fringing field and the effective length of quadrupoles and bending magnets," (in preparation, Stanford Linear Accelerator Center, Stanford University, Stanford, California).
5. S. Butterworth, "Alternating current resistance of solenoidal coils," Proc. Royal Soc. (London) 107, 693 (1925).
6. H. Brechna, "Some aspects of modern transformer core design," Bulletin Oerlikon 324, 70-78 (October 1957).
7. H.S. Carslaw and J.C. Jaeger, Conduction of Heat in Solids (Oxford University Press, 1959).
8. H. Brechna, "Erwaermung und Kuehlung der Eisenkoerper von Leistungstransformatoren," Neue Technik Nos. 4 and 5 (1960).
9. W. Rohsenow and H. Choi, Introduction to Heat, Mass and Momentum Transfer (Prentice-Hall, New York, 1961); p. 196.
10. H. Brechna, "Einfluss von Form und Bauart der Transformatoreisenkoerper auf die Ummagnetisierungs verluste," Scientia Electrica, Vol. V (1959).
11. F. E. Terman, Radio Engineers Handbook (McGraw-Hill Book Company, New York, 1943).
12. A.E. Knowlton, Standard Handbook for Electrical Engineers (McGraw-Hill Book Company, New York, 1957); Sections 23-127.
13. H. Jordan, "Angenaeherte Berechnung des Magnetischen Geraeusche von Kaefiglaeufermotoren," E.T.Z. 71, 491 (1950).
14. W. H. McAdams, "Heat transmission," Chemical Engineering Series, McGraw-Hill Book Company, Inc., New York (1954).